High-resolution liquid- and solid-state nuclear magnetic resonance of nanoliter sample volumes using microcoil detectors

A. P. M. Kentgens,[1,a)] J. Bart,[2] P. J. M. van Bentum,[1] A. Brinkmann,[1] E. R. H. van Eck,[1] J. G. E. Gardeniers,[2] J. W. G. Janssen,[1] P. Knijn,[1] S. Vasa,[1] and M. H. W. Verkuijlen[1]
[1]*Institute for Molecules and Materials, Radboud University Nijmegen, Toernooiveld 1, 6525 ED Nijmegen, The Netherlands*
[2]*MESA+ Institute for Nanotechnology, University of Twente, P.O. Box 217, 7500 AE Enschede, The Netherlands*

(Received 26 November 2007; accepted 17 December 2007; published online 23 January 2008)

The predominant means to detect nuclear magnetic resonance (NMR) is to monitor the voltage induced in a radiofrequency coil by the precessing magnetization. To address the sensitivity of NMR for mass-limited samples it is worthwhile to miniaturize this detector coil. Although making smaller coils seems a trivial step, the challenges in the design of microcoil probeheads are to get the highest possible sensitivity while maintaining high resolution and keeping the versatility to apply all known NMR experiments. This means that the coils have to be optimized for a given sample geometry, circuit losses should be avoided, susceptibility broadening due to probe materials has to be minimized, and finally the B_1-fields generated by the rf coils should be homogeneous over the sample volume. This contribution compares three designs that have been miniaturized for NMR detection: solenoid coils, flat helical coils, and the novel stripline and microslot designs. So far most emphasis in microcoil research was in liquid-state NMR. This contribution gives an overview of the state of the art of microcoil solid-state NMR by reviewing literature data and showing the latest results in the development of static and micro magic angle spinning (microMAS) solenoid-based probeheads. Besides their mass sensitivity, microcoils can also generate tremendously high rf fields which are very useful in various solid-state NMR experiments. The benefits of the stripline geometry for studying thin films are shown. This geometry also proves to be a superior solution for microfluidic NMR implementations in terms of sensitivity and resolution. © *2008 American Institute of Physics*. [DOI: 10.1063/1.2833560]

I. INTRODUCTION

Sensitivity is the Achilles' heel of nuclear magnetic resonance (NMR). Despite the fact that NMR probes local interaction and can therefore provide structural information on the subnanometer scale, it can only do so if at least tens of milligrams of sample exhibiting that structure is available. This is due to the very low energies that are involved in the nuclear spin transitions. Even at the highest possible magnetic fields the Zeeman splitting is much lower than the thermal energy k_BT at room temperature. As a result the various spin states are almost equally populated. This puts severe constraints on the applicability of NMR in a number of research fields. High-resolution NMR analyses can be problematic for natural products which can only be extracted in minute quantities. The same is true for high-throughput screening or the *in situ* study of reactions in "lab on a chip" type applications. In solid-state NMR bottlenecks are encountered if limited amounts of biological materials or precious minerals are available. This problem is aggravated if specific sample geometries are of interest such as small single crystals, thin films, or fibers. E.g., for self-assembling functional materials there may be bulk quantities of the starting material present but the specific functionalized molecular assembly generally comes only in nanoliter quantities.

Considering the potential of NMR in terms of providing local structural information and insight into molecular dynamics, method development has been focused mainly on devising new pulse sequences that make it possible to either average or (re-)introduce certain parts of the spin Hamiltonian so that structural information can be extracted in a clear and unambiguous way. Now that the majority of these techniques have come to maturity and NMR has established its reputation as one of the most versatile analysis techniques, one observes a surge of interest for sensitivity enhancement methods as is also evidenced by various contributions in this issue.

The most promising approach is to prepolarize the spin system by polarization transfer. The majority of experiments on low gamma nuclei involve transfer of polarization from abundantly present proton spins which have a much larger Zeeman splitting, allowing an enhancement proportional to the ratio of the gyromagnetic constants. Since the electron magnetic moment is much larger than any nuclear moment, exploiting the coupling of the nuclear spins to unpaired electron spins can be very advantageous. This dynamic nuclear polarization (DNP) phenomenon is being investigated with varying intensity. Shortly after discovery of NMR the trans-

a)Electronic mail: a.kentgens@nmr.ru.nl.

fer mechanisms, such as the nuclear Overhauser effect[1] or the solid effect, underlying various forms of polarization transfer were described.[2]

With the advent of high-resolution solid-state NMR, DNP research reemerged and focused on the investigation of materials where unpaired electrons are inherently present such as diamonds, coal, chars, doped organic polymers, etc.[3] With the drive to higher external NMR fields the interest for DNP declined, however, since the strengths of the main polarization transfer effects become less efficient at higher magnetic fields. Moreover there was no clear strategy to make DNP more generally applicable to materials without unpaired electrons. It was the pioneering work of Griffin and co-workers that changed this situation by introducing suitable microwave sources[4,5] for high-field DNP-NMR, optimizing sample preparation techniques using frozen solutions containing radicals,[6] and studying the transfer mechanisms that can be exploited at high fields.[7] This knowledge is now exploited in the development of new radicals and radical mixtures that optimize the transfer efficiency using three-spin processes.[8,9] Inspired by the DNP work on frozen solutions Ardenkjaer-Larsen *et al.*[10] developed a protocol to quickly dilute these solutions after DNP enhancement to produce highly polarized molecules to be used in liquid-state NMR and specifically *in vitro* and *in vivo* applications. This approach, which will lead to many practical applications and trigger further methodological investigations, has been commercialized. A more attractive approach to working with permanently present unpaired electrons, which can have a detrimental effect on spectral resolution, would be to temporarily create them, e.g., by optically exciting electron spins into triplet states.[11,12] This has proven to be difficult to harness in high-resolution NMR, however.[13] In semiconductors optically enhanced polarization due to photoexcited spin-polarized electrons is more readily observed,[14] but transfer of this polarization to (deposited) organic or biological compounds has not been taken up yet.[15,16]

In liquids, nuclear hyperpolarization by *chemically* induced radical pairs has proven to be much more accessible.[17–19] This chemically induced dynamic nuclear polarization (CIDNP) has been used extensively to study chemical reactions forming radical intermediates.[20] By probing (changes in) the solvent accessibility of tryptophan, tyrosine, and histidine residues in proteins by means of laser-induced photochemical reaction information about the folding of proteins can be obtained.[21,22] More recently photo-induced polarization has also been explored in photosynthetic reaction centers in solid-state NMR.[23,24] Ongoing research by Diller *et al.* gives insight in the mechanisms involved.[25] This holds some promise as an alternative polarization source if synthetic photoreaction centers can be made.

Another promising chemical approach to produce highly spin-polarized molecules is the use of parahydrogen ($p\text{-}H_2$) in hydrogenation reactions performed either in high field[26] or zero field with subsequent cycling to high field.[27] Parahydrogen (hydrogen with the coupled proton spins in the singlet state) is stable in liquid solutions and can be used as a fully spin-polarized reactant. In most hydrogenation reactions the symmetry of the proton pair will be broken leading to highly spin-polarized reaction products giving strongly enhanced spectral NMR resonances. This can be used not only to identify reaction intermediates and study the reaction kinetics but also to produce polarized molecules which can subsequently be used in *in vitro* or *in vivo* magnetic resonance spectroscopy and imaging experiments.[28–30]

In solids a more exotic mechanism to exploit the spin statistics of indistinguishable protons is the Haupt effect.[31,32] In this case the coupling of methyl rotational states to the nuclear spin states at low temperatures is exploited. After a fast temperature jump, the rotational states can fully thermalize only by inducing nuclear spin flips. The rotational states equilibrate fast within the different proton isomers but cross relaxation is much slower leading to a cooling of the spin system.[33,34]

Finally, in the gas phase one can use the selection rules of optical transitions in alkali metals to spin-selectively-pump an atomic transition. In diluted gases this spin polarization can be transferred by collisions to noble gases such as ^{3}He or ^{129}Xe.[15] This is the most developed polarization enhancement technique where the high degree of polarization is combined with the sensitivity of the ^{129}Xe chemical shift for its direct surroundings.[35] Being a gas ^{129}Xe NMR is used extensively to study meso- and microporous solids such as heterogeneous catalysts[36] or polymers.[37] Because of its binding to lipids and proteins ^{129}Xe NMR has also been targeted for biological applications.[38] Trapped in cryptophane-A cages it can be used as a biosensor.[39,40] Hyperpolarized gases are also very popular in magnetic resonance imaging (MRI),[41] where ^{3}He is especially interesting for lung imaging.[42] Transferring the polarization to other compounds using cross polarization or spin polarization-induced nuclear Overhauser effect (SPINOE) (Ref. 43) has not found widespread application. In the low-temperature regime residence time of the xenon is long enough that the study of crystal surfaces becomes feasible, however.[44]

As has been summarized above great progress has been made in the various approaches to enhance the NMR spin transitions by establishing non-Boltzmann populations in the spin system. So far, however, there is no generic protocol that can be used to spin polarize any substance. In fact, most solutions described above only work for certain classes of material and need substantial investment in additional hardware. Therefore it is of interest to explore alternatives such as optimizing the currently used detector technology for mass-limited samples. Even if the potential gains are much smaller it should be realized that a signal gain of a factor of 10 will bring down experiment time by a factor of 100 which can easily bring the measurement times for various experiments so far considered impossible down to a feasible level.

Presently, the predominant means to detect NMR is to monitor the voltage induced in a radiofrequency coil by the precessing sample magnetization. As has been reviewed by Webb,[45] using the Hoult–Richards approach[46] to describe the signal-to-noise ratio in an inductively detected NMR experiment, the sensitivity of a solenoid NMR coil is inversely proportional to the coil diameter given a constant length-to-diameter ratio. In 1994 Webb and co-workers demonstrated

that by miniaturizing the detection coil, the NMR sample volume could be brought down to the nanoliter regime.[47,48] This has triggered substantial research into the use of microcoils (loosely defined here as coils with less than 1 mm diameter) mainly in liquid-state high-resolution NMR as has been reviewed recently by Webb.[49] In liquid-state NMR two different approaches toward miniaturization are pursued: one focuses on capillary NMR,[50,51] where tightly wound solenoids are the predominant coil design and the second approach is to work in microfluidic devices which use planar helical structures for the detection of the NMR signal.[52–55] Of considerable interest for liquid-state NMR is the hyphenation with other analysis and microseparation techniques such as liquid chromatography, electrophoresis, and even gas chromatography.[56–59]

Although making smaller coils seems a trivial step, the challenges in the design of microcoil probeheads are to get the highest possible sensitivity while maintaining high resolution and keeping the versatility to apply all known NMR experiments. This means that the coils have to be optimized for a given sample geometry, circuit losses should be avoided, susceptibility broadening due to probe materials has to be minimized, and finally the B_1-fields generated by the rf coils should be homogeneous over the sample volume. Moreover, the rf circuit should be simultaneously tunable for multiple frequencies to allow multinuclear experiments. The basic considerations for solenoid microcoils have been reviewed by Webb.[45] Optimization of rf homogeneity and signal-to-noise ratio is treated by Minard and Wind;[60,61] they gave clear guidelines for the design of solenoid microcoils with respect to the number of windings and wire diameters depending on the conductivity of the samples. Engelke has described the specific problems that are encountered in the high-frequency operation of solenoid coils where the wavelength of the rf irradiation is no longer large with respect to the coil dimensions.[62] Eroglu *et al.* have specifically analyzed the design parameters for flat helical coils, in particular, for use in microfluidic devices, showing that high volume/mass sensitivity is achievable at moderate spectral resolution as the close proximity of the coil to the sample degrades the local B_0-field homogeneity.[63]

Considering the amount of work in the field of high-resolution liquid-state NMR it is surprising to see that there has been relatively little research toward the possible use of microcoils in solid-state NMR. Favorable characteristics of solid-state NMR in this respect are that the demands for spectral resolution are somewhat relaxed and that in many cases the spin density of the sample is relatively high. Technically involved is the fact that the sample has to be spun at the magic angle to obtain isotropic spectra for powdered samples.

This contribution reviews the current state of the art of microcoil solid-state NMR with some emphasis on our efforts in the development of static[64] and micro magic angle spinning (microMAS) solenoid-based probeheads[65] and the development of static probes optimized for thin films. For the latter application the stripline geometry,[66,67] which also proves to be a superior solution for microfluidic NMR implementations as will be discussed, has been introduced.

II. SENSITIVITY CONSIDERATIONS

The motivation to miniaturize the receiver coil is based on the principle of reciprocity as introduced by Hoult and Richards.[46] As stated in the didactical reviews by Hoult[68,69] this means that the B_1-field created at the NMR sample by applying a certain current to the NMR receiver coil is proportional to the signal strength induced in the coil by the precessing magnetization M in the sample during signal detection. In other words, a coil that generates a high B_1-field per unit current is also a sensitive detection coil. This also implies that one needs to put the sample at the position where the coil concentrates most of its magnetic energy.

Based on these considerations starting from the magnitude of the magnetization M_0 per unit volume, given by Curie's law in the high-temperature limit,

$$M_0 = N\gamma^2\hbar^2 I(I+1)\frac{B_0}{3k_B T}, \tag{1}$$

where N is the number of spins per unit volume, γ the gyromagnetic ratio, I the spin quantum number, B_0 the static field, T the temperature, and h ($\hbar = h/2\pi$) and k_B are Planck's and Boltzmann's constants, respectively; the signal-to-noise ratio in the receiver coil can be deduced. The signal s induced in the coil due to the precessing magnetization m in an infinitesimal volume at position r in the coil is

$$s \sim -\frac{d}{dt}\left(\frac{B_1(r)}{i}m(r,t)\right), \tag{2}$$

where $B_1(r)/i$ is the magnetic field induced in the rf coil per unit current. Using the expression for the thermal noise in an electrical conductor $N_R = \sqrt{4k_B TR\Delta f}$ with Δf being the spectral bandwidth and R is the resistance due to conductive losses in the coil and sample, integrating over the whole sample volume the signal-to-noise ratio of the NMR experiment is obtained:

$$\frac{\mathrm{S}}{\mathrm{N}} = \frac{k_0\left(\frac{B_1}{i}\right)V_s N\gamma\hbar^2 I(I+1)\frac{\omega_0^2}{k_B T 3\sqrt{2}}}{F\sqrt{4k_B TR\Delta f}}, \tag{3}$$

where k_0 is a scaling factor accounting for the rf inhomogeneity of the coil, V_S the sample volume, ω_0 the nuclear Larmor precession frequency, and F the noise factor of the spectrometer. It is assumed implicitly in this derivation that the dominating noise sources are the coil and possibly the sample but not the preamplifier. In that case the quality factor Q of the LC circuit does not enter into the equation since both signal and noise are amplified by the same amount. From Eq. (3) the possibilities to optimize sensitivity are easily identified. The obvious choice is to go to the highest possible external field to maximize ω_0; furthermore, it is advantageous to cool the detector circuitry as is done in so-called cryoprobes to reduce the noise and if possible cool the sample leading to a reciprocal increase in the magnetization. In terms of the design of the detector coil one should optimize the filling factor and as stated by the reciprocity theorem design the coil such that the highest possible rf field is generated per unit current, i.e., maximize B_1/i. It goes with-

out saying that one should minimize all possible losses in the rf circuit as the actual signal-to-noise (S/N) ratio is proportional to $S/N \sim B_1/i\sqrt{R}$. The length of coil wire should be short with respect to the rf wavelength to generate a uniform B_1-field.[62,69] The coil geometry is an important design parameter to get high sensitivity; to get the optimal S/N ratio the coil design has to be adapted to the specific size and shape of the sample, generating a high (and for most experiments uniform) B_1-field at the site of the sample. For a high effective filling factor the integrated magnetic energy ($\sim \int B_1^2 dV$) outside the sample should be as low as possible. A more extensive set of guidelines for coil design can be found elsewhere.[66]

III. COIL GEOMETRY

A. Helical

In solid-state NMR the solenoid coil is the predominant coil geometry. From textbook physics it is well known that tightly winding a long wire in the form of a helix is an efficient way to produce a strong and nearly uniform field in the coil interior. For solid samples such as powders or single crystals in a cylindrical sample holder this is a convenient geometry as the coil can be tightly wound around the sample holder providing a good filling factor. It also provides an obvious symmetry for sample rotation around an axis, e.g., for crystal rotation studies or magic angle spinning. Note, however, that about half of the magnetic energy is outside the coil which puts an upper limit to the efficiency. The B_1/i factor of the solenoid is very good; it does not only ensures a high detection sensitivity but also makes it possible to generate very large rf fields which are, e.g., useful for the excitation of very broad spectra. The center field of a cylindrical coil can be deduced using Biot–Savart's law as follows:

$$\frac{B_1}{i} = \frac{\mu_0 n}{2r} \frac{1}{\sqrt{1 + (l/2r)^2}}, \tag{4}$$

where μ_0 is the permeability of free space, n the number of turns in the coil, and r and l the radius and length of the coil. Equation (4) makes it clear that sensitivity increases with the inverse of the diameter for coils with a fixed form factor $l/2r$, which is the basic rationale for using microcoils to get NMR spectra from mass/volume-limited samples. Even for an ideal solenoid the B_1-field falls off to half the center field at the ends of the helix. This inherent rf inhomogeneity is amplified by the fact that parallel currents repel each other, leading to a redistribution of the current away from the axis for the outermost windings. The decrease in rf-field strength at the edge of the coil can be somewhat counteracted by reducing the winding pitch at the end of the coil (so-called end-compensated coils).[70] Solenoids can be miniaturized relatively easy to coil diameters of about 100 μm as has been demonstrated in various designs aiming at different liquid and solid NMR applications.[64,65,71–76] As the wire diameters become very small this is a delicate job and the resulting coils are extremely fragile. Wire with diameters down to ~25 μm is commercially available. Scaling down a solenoid with a constant form factor hardly affects its resistance as long as the wire diameter is large with respect to the penetration depth of the rf radiation.[77] Considering the small dimensions of the coil extra care must be taken to avoid signal losses due to the leads connecting the coil to the circuit. Furthermore these leads break the symmetry of the coil adding to the rf inhomogeneity. General design guidelines in terms of coil length depending on the required homogeneity, wire diameter, and number of windings have been formulated by Minard and Wind[60,61] for both lossy and nonlossy samples.

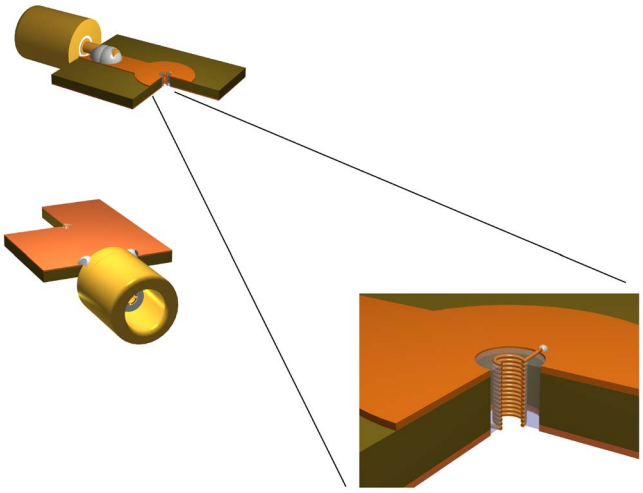

FIG. 1. (Color online) Illustration of the microcoil integrated in a high-frequency laminate which can easily be integrated in tuning circuit without introducing resistive losses due to connecting leads. This also provides good thermal anchoring for the coil.

We introduced the design shown in Fig. 1 to minimize most of the problems of the microsolenoids.[64] The crucial innovation of this design is to embed the helix in the center of a custom-made capacitor disk, which provides an *LC* geometry with very short connections. This minimizes the resistive rf losses and provides a good thermal anchoring of the coil. Since the currents in the capacitor plates are essentially radial, a minimum distortion of the rf field pattern is achieved. Furthermore this gives the design the mechanical rigidity to be able to load and unload samples without breaking the coil. The microcoil itself is wound on a vespel coil former with a thread that is cut on a computer numerical control (CNC) lathe. This also allows for the implementation of end compensation if needed. To further improve the filling factor in the newest design the microcoil is fixed inside a quartz sleeve making a coil former on the inside of the coil no longer necessary (Fig. 2). The coil in its sleeve is embedded in a custom-made circuit on a high-frequency laminate. Coils down to 200 μm have been constructed being efficient detectors for single crystals and powders in the nanoliter/microgram regime.[64] The geometry is also favorable to study oriented fibers.[78] By mounting this circuit on a macroscopic MAS stator it proved possible to construct piggyback magic angle spinning probeheads[65] (see below) allowing high-resolution solid-state NMR for samples where only several micrograms of material are available (see below).

B. Flat helical

Many interesting solid samples are grown as thin films, coated onto a surface, or oriented on glass plates such as

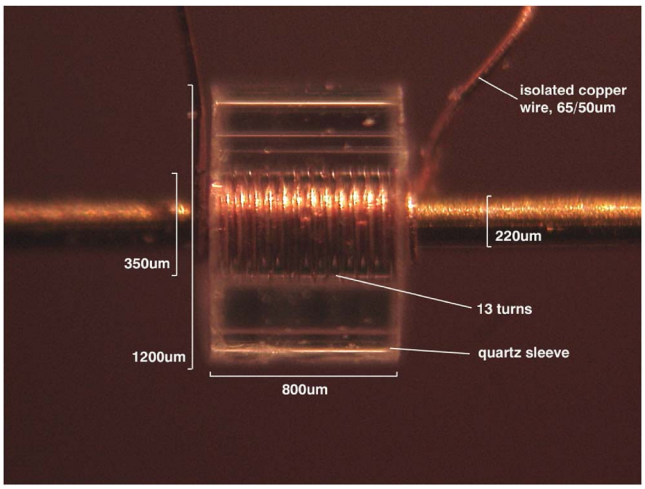

FIG. 2. (Color online) Actual photograph of the microcoil production, indicating the dimensions of the coil. The microcoil consisting of a 50 μm insulated copper wire is tightly wound on a 220 μm wire, and inserted in a quartz sleeve to provide mechanical rigidity.

lipid bilayers. A solenoid is not well adapted to that geometry and alternative coil forms are needed to be able to investigate such samples by NMR. Flat rectangular solenoid coils have been introduced in which it is possible to stack aligned lipid bilayer samples on glass plates.[79,80] This approach still needs a substantial amount of sample and the possibility to stack a large number of surface layers. To study thin films in their actual setting a planar detector is necessary preferably scalable to the available sample dimensions. Planar coils are very common for localized MRI and again spiral design is the most common geometry. As standard lithography techniques can be used to define structures with dimensions down to below 1 μm it is possible to scale down flat helical coils to very small dimensions. A typical coil layout with the corresponding rf field profile is shown in Fig. 3. A detailed analysis of such a surface spiral, as shown in Fig. 4, indicates that this design has some serious drawbacks, however. First, every winding that is added is less efficient than the previous one as it contributes less to the center axial field but it increasingly adds to the resistive losses in the coil. Second, the fields produced by the outer windings cause considerable eddy currents in the center windings adding additional losses and lowering the field homogeneity in the center region. Therefore the optimum for a flat helix is found for a single or a few windings depending on the optimization of high B_1-field versus optimum sensitivity. A third disadvantageous aspect of surface coils is that the innermost winding has to be connected to the contact pads via a bridge. This not only further disrupts the rf homogeneity but also complicates production with the need of extra layers and thus introducing additional losses. Nevertheless efficient detectors can be made in this way. Besides for imaging purposes this coil type has been put forward for use in microfluidic devices where one also needs flat structures.[52–55] The calculation of the B_1/i and the coil resistance of this design, together with an analysis of the sensitivity as function of the number of windings has been given by Eroglu *et al.*[63]

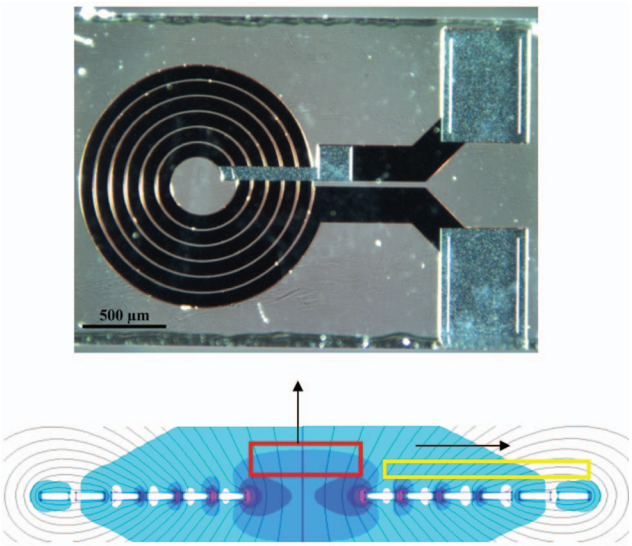

FIG. 3. (Color) Planar microcoil with six windings, inner diameter 300 μm, and outer diameter 1.4 mm. The bridge necessary to connect the inner winding to the contact pad is clearly visible. The rf-field intensity is represented in a colormap. The red box points out the volume that is commonly used for NMR with the B_1-field pointing in the axial direction. Above the wire the B_1-field mostly points in the radial direction (yellow box). Adapted from Ref. 66.

C. Stripline

The only requirement for NMR excitation and detection is that a sufficiently strong B_1 component is generated perpendicular to the static B_0-field and therefore any structure is allowed. From textbook physics it is known that running a current i through a straight wire will generate a cylindrical B_1-field around this wire. With the wire parallel to the external field direction the B_1-field is oriented perpendicular to the external static field at all positions in space and can thus be used to excite a NMR transition. By reciprocity the same wire can be used to detect the NMR signal. It should be realized that because B_1 points in different directions in space, the spins do not have a uniform precession in space after a pulse has been applied. Nevertheless they all contribute in phase to the induction voltage across the wire as indicated by Eq. (2). Clearly a simple wire is not an efficient NMR detector as the rf-field strength decays inversely with the distance to the wire. This can be remedied to some extent by putting a cylindrical conductor around the wire as in coaxial arrangement. This geometry indeed results in a sensitive NMR detector as used in toroid cavities.[81] For regular NMR its drawback is the remaining strong rf inhomogeneity; this can be exploited favorably, however, in imaging and diffusion experiments.[82,83]

The stripline can be seen as a two-dimensional analog of such a coax line. In a stripline the current is fed through a thin metal strip. A nonradiative closed configuration is realized by placing ground planes both above and below the strip. The magnetic field lines encircle the central strip as is shown in Fig. 5. The B_1-field points in opposite directions above and below the stripline but, as in the case of the single wire, sample put at both sides of the strip will contribute in phase to the signal. The boundary conditions at the metal surface dictate that the field lines run parallel to this surface;

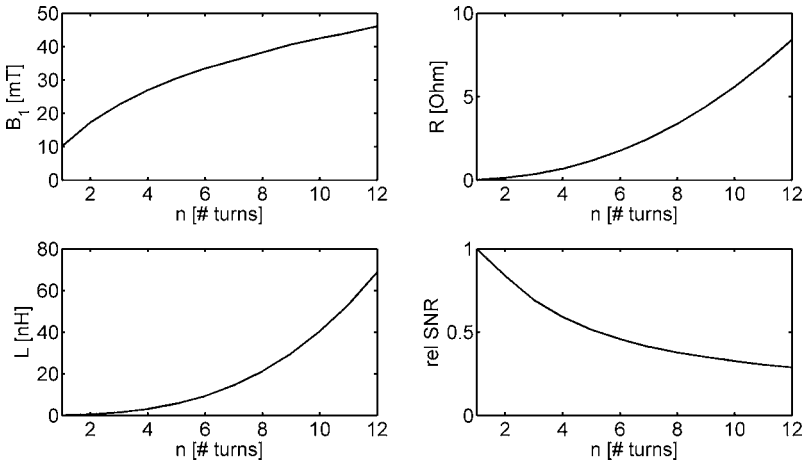

FIG. 4. Analysis of an idealized planar microcoil with an inner diameter of 100 μm and a spacing of 13.2 μm between the windings. The effect of adding concentric windings is analyzed analytically based on Biot–Savart's law. The width and height of the copper deposits are taken to be 40×20 μm^2. Adding more windings increases B_1/i in the center of the field but the signal-to-noise ratio for a given number of spins goes down as each new winding introduces more resistive losses and has a relatively low filling factor (see text).

as a result a very good B_1-field homogeneity is realized. Our stripline design[67] is based on quarter or half wavelength resonators (Fig. 5) that can in principle be constructed on a chip with no discrete soldered elements in the resonating circuit. In comparison with the planar helix the stripline has the advantage that all connections can be made in the same plane, removing the problems associated with the connection to another plane. The current distribution over the strip is fairly homogeneous except at the very edges, and eddy currents are avoided. By analytically evaluating the expressions for B_1/i and the resistance R of a cylindrical current shell and a stripline of equal volume one finds that the signal-to-noise ratio can be a factor $\sqrt{2}$ better for the stripline. Numerical finite element calculations find a similar sensitivity relation for the different geometries.[67] A very interesting feature of the stripline design is that the surface can be scaled in a simple and trivial way so that optimal matching for specific sample sizes is feasible.

Striplines and microstrips (which have only one ground plane) are very popular as transmission lines in integrated microwave circuits. So far there has been one account of using microstrips to build square surface coils for MRI.[84] Recently Maguire *et al.* introduced the microslot design that bears common ideas to the stripline design.[85] In both cases the sample sits close to a small metal strip carrying the rf current. In the microslot design no attempt is made to homogenize the B_1-field as ground planes are absent. Both designs give some very promising results both in terms of sensitivity and resolution.

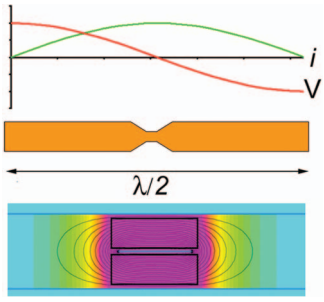

FIG. 5. (Color) Illustration of the stripline design. In the $\lambda/2$ configuration the current maximum is in the middle. Due to the constriction the current density will be strongly enhanced. As is shown in the cross section by sandwiching the strip between two ground planes a volume with a high a uniform and high B_1-field is created, ideal for high-sensitivity NMR.

Finally, a point of concern in NMR of biological samples is the dielectric sample heating due to rf currents induced in the sample. Here again the stripline is a favorable configuration especially when designed as a $\lambda/2$ mode structure (Fig. 5). In this case the electrical field is zero at the center of the strip due to the symmetry of the design. Furthermore, the surface area and the dielectric material can be chosen to provide optimum cooling if long and intense rf irradiation of the samples is necessary. Numerical simulations have shown that for liquid aqueous samples the maximum electrical fields near the ends of the central stripline are about a factor of 10 lower than in a comparable helix that generates the same B_1-field. A detailed analysis and design guidelines are given by van Bentum *et al.*[67]

Figure 6 shows an interesting comparison of the solenoid, flat helical, and stripline detector, comparing the size of the design within an effective sample volume of 5 nl. This volume is defined rather arbitrary as the volume in which B_1 is within 10% of the maximum value in the center of the coil. As can be seen the stripline provides the most compact design as it has the highest effective homogeneous B_1 volume. As a result it also gives the highest sensitivity. A numerical analysis of the designs for proton NMR at 600 MHz predicts that, respectively, 3×10^{12}, 7×10^{12}, and 4×10^{12} proton spins/$\sqrt{}$Hz would be needed for the stripline, the flat helical

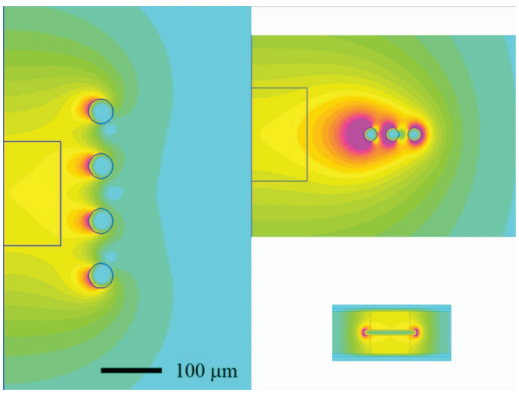

FIG. 6. (Color) Comparison of the sizes of a solenoid, a flat helical, and a stripline design needed for NMR experiments on 5 nl of sample. The sample is confined to a volume where the B_1-field varies by less than 10%. For the helical probes this sample volume is cylindrical. The scalability of the stripline allows for a compact design with the sample in rectangular bars of 1 mm long.

coil, and the solenoid to generate a S/N ratio of 1 in a single scan. This is the definition adopted here to express the "limit of detection" (LOD); the number of spins that have to resonate in 1 Hz bandwidth to give a signal as strong as the noise in single acquisition. Practically, the limit of detection for a given sample-detector combination will depend on the linewidth, the spectral bandwidth, and the amount of time available to signal average.

IV. RESOLUTION

Although microcoils have great advantages in terms of sensitivity and excitation bandwidths, they have not yet been embraced as a general tool in mainstream NMR research. This is mostly due to the compromises that must be made in spectral resolution. High sensitivity demands a high filling factor, so the sample will be in close contact with the rf coil. In general the magnetic susceptibility of the metal wire will be different from that of the coil former (or air in a freestanding coil) and the sample holder; as a result local variations of the static magnetic field occur in the sample which reduces the spectral resolution. The small dimensions of the microcoil lead to field gradients that vary over very short distances and the resulting field profile cannot easily be shimmed by macroscopic shim coils far away from the sample.

A uniform, infinitely long, cylinder oriented perpendicular to the magnetic field will have a uniform field in its interior.[45] This situation can be mimicked by immersing the coil in a medium that have the same susceptibility as a copper metal.[48] Some perfluorocarbons that have volume susceptibilities close to the copper susceptibility are available. These perfluorocarbons introduce no proton background signal. In fact, this solution has found its way into commercial microcoil probes for capillary NMR. The successful susceptibility matching of these solenoidal coils has led to extensive applications, for example, in the field of high-throughput screening.

An alternative is to use zero susceptibility wire to avoid deterioration of the spectral resolution due to the close proximity of the coil to the sample. Zero-susceptibility wire is produced from a coaxial structure of metals which have opposite signs in susceptibility such as copper and aluminum. The thickness of the layers has to be accurately controlled so that the metal volumes are consistent with the ratios of the volume susceptibilities.[45,86] Again susceptibility matched coils have found their way into a number of homebuilt and commercial probes showing that high resolution close to that in regular liquids probes is possible using solenoid microcoils if adequate measures are taken.[49] For planar helical coils the ultimate resolution has not yet been achieved, however.

In contrast to helical coils, the stripline has some properties that make the susceptibility problem much easier to handle. The first aspect is that the axis of the stripline can be oriented parallel to the static field B_0. The magnetization of the copper strip is homogeneous and oriented parallel to the external field. From Maxwell's equations it is easy to see that for an infinitely long strip, there is no field inhomogeneity at the position of the sample and thus the ultimate resolution

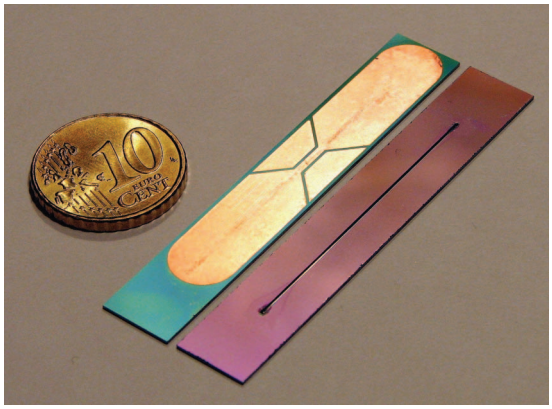

FIG. 7. (Color) Photograph of the two halfs of a microfluidic NMR chip based on the stripline design showing the copper construction of the $\lambda/2$ resonator on one half and the microfluidic channel on the other half. The two halfs are bonded together in the final device.

provided by the magnet should be attainable. Calculation of the local field variations for a plane just above a stripline shows that the susceptibility broadening can be limited to below 0.1 ppm.[67] Furthermore, it is not necessary to etch all copper to construct the narrow strip section. Etching a narrow line as shown in Fig. 7 suffices, which means a minimal disruption of a long uniform strip. As will be shown in Sec. VII this approach is very effective and a resolution of 1 Hz is achieved for protons at 600 MHz. A similar figure is reported by Maguire *et al.* for the microslot design.[85]

V. CIRCUIT DESIGN

As microcoils have a low inductance and a low resistance, special attention is needed in the circuit design. Losses at the coil contacts should be minimized. One way to achieve this is by embedding a solenoid coil in an external capacitor. In the earliest single-tuned versions of this probe design, the coil-capacitor circuit was resonant and coupled capacatively to the matching circuit.[64] For double-tuned probeheads this proved to be less convenient. The rf circuit as used in our latest double-tuned microMAS probehead is shown in Fig. 8. The microcoils' low inductance, combined with the low resistive loss factor, allows for a relatively high Q operation. A conventional LC resonator circuit is not well adapted for very low impedance coils and we have chosen to implement a standing wave resonator for the proton channel. In this case it is a free space coaxial $\frac{3}{4}$ lambda structure with the coil acting as a short on one side. Tuning of the ^{1}H resonator is accomplished by shifting a dielectric sleeve into the coaxial structure. The open end of the coaxial resonator is capacitively coupled and matched to the external 50 Ω circuit. The X channel is based on a conventional LC circuit with a trap that blocks the high-frequency proton signals from entering the X channel. The summing point is chosen inside the coaxial resonator at a node in the proton standing wave, where the ^{1}H electrical rf field is close to zero. At that point the influence of the X channel on the ^{1}H channel is negligible. The measured Q factors for this probe circuit depend on the operating frequency and are respectively, about 50 for ^{1}H and 20 for the X channel tuned on ^{13}C.

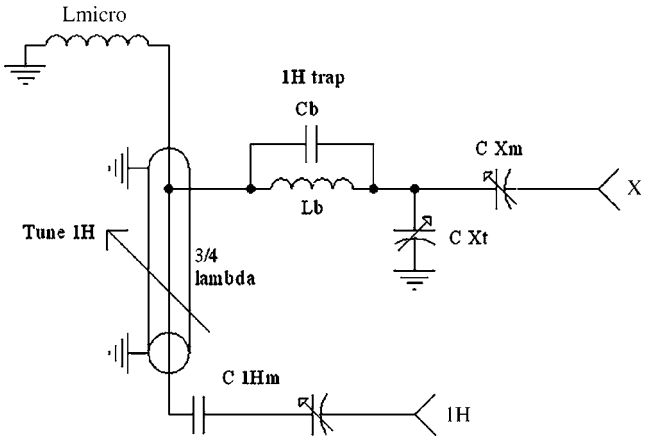

FIG. 8. Electrical circuit for a double-resonance H*X* microMAS probehead. The ^{1}H resonator is a free space coaxial $\frac{3}{4}$ lambda structure with the coil acting as a short on one side. Tuning is accomplished by moving a dielectric sleeve in the coaxial structure. The open end of the coaxial resonator is capacitively coupled and matched to the external 50 Ω circuit. The *X* channel is based on a conventional *LC* circuit with a trap that blocks the high-frequency proton signals from entering the *X* channel.

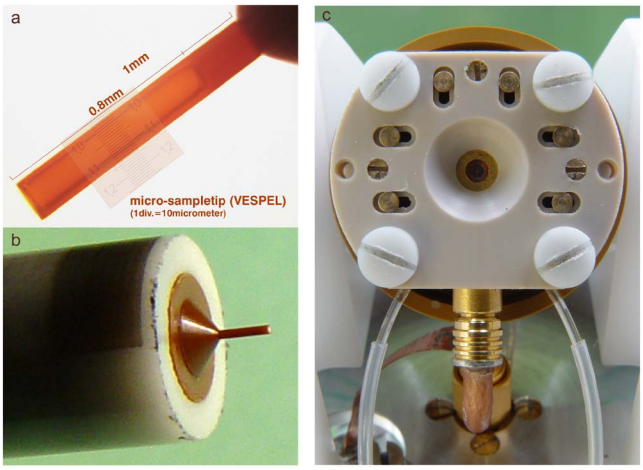

FIG. 9. (Color online) (a) Micrograph of the microrotor indicating its inner and outer dimensions. (b) Photograph of the microrotor tip inserted into the regular MAS rotor. (c) Photograph of the microcircuit holder placed on the MAS stator showing the sliders and screws used to align the microcoil circuit with respect to the microrotor.

The stripline probeheads are constructed with the strip either being a $\lambda/4$ or a $\lambda/2$ circuit.[67] A prototype probehead with a 1 mm long stripline with a width of 500 μm was produced photolithographically using low-loss Teflon-based printed circuit board material to produce a $\lambda/4$ structure for protons. The stripline is inserted as a short at one side of the resonator and a capacitive coupling and tuning network near the open side of the resonator. The coupling to the $\lambda/4$ resonator is chosen at a convenient point to achieve the best matching conditions. Tuning is realized by the insertion of variable length dielectric stubs inside the coaxial resonator structure. Double tuning is achieved by coupling a second coaxial resonator structure using a proton trap to avoid high-frequency coupling into the *X* channel. Typical *Q* factors for this design are between 80 and 100. The $\lambda/2$ resonators, as used in our microfluidic device, are fully defined in planar lithography and embedded in a single chip. This resonator is capactively coupled to the external (fine) tuning and matching circuit. Here the resonators' *Q* is influenced by material properties and amounts to about 50.

VI. MAGIC ANGLE SPINNING

The two cornerstones of the success of NMR as an analytical tool for the study of solid materials in the widest sense are double resonance and magic angle spinning. The possibility to transfer polarization from abundant nuclei (e.g., protons) to less abundant nuclei with low gyromagnetic ratios such as ^{13}C or ^{15}N helps us to relieve sensitivity problems which are particularly important for mass-limited samples. Moreover, double resonance can be used to determine the spatial proximity between different types of nuclei and is therefore an important tool to provide structural information. To obtain high-resolution spectra, sample rotation about the "magic angle" is imperative to average anisotropic contributions to the resonance lines.[87,88] The evolution of a variety of techniques for studying internuclear distances, bond angles, molecular orientation and/or dynamics, spin diffusion, and chemical exchange processes is built on this foundation.

As was described in the previous section circuit designs allowing double and possible triple tuning of the probeheads can be envisioned. Spinning a microsized rotor with a diameter well below 1 mm at high speed inside a small diameter microcoil is not so obvious, however. A freestanding microrotor is a very delicate object which is difficult to handle. It proves to be tedious to further miniaturize the current double-bearing MAS stators to rotor sizes below 1 mm especially when a proportionally increasing spinning speed is desired.[89]

We devised a design where the microrotor is piggybacked on top of a regular commercial MAS rotor (Fig. 9). For the rf circuit a microcoil-based resonator, with a solenoid coil integrated into a high-frequency laminate as was described above, is used. The advantage of this design is its mechanical stability and minimization of signal losses. The circuit is mounted on top of a commercial MAS stator. Alignment to the microrotor is critical as the inner coil diameter is 220 μm whereas the microrotors' outer diameter is 170 μm leaving only 25 μm of free space between rotor and coil. This alignment is achieved by optically aligning the circuit with respect to a spinning rotor and then fixing it on top of the stator [Fig. 9(c)]. We found spinning to be remarkably stable without any sizable excursions of the rotation axis; as a result the attainable spinning speeds are those imposed by the macrorotor. It is worth noting that so far no rotors were broken during spinning. Sample handling and filling prove to be the most critical steps in setting up experiments.

Piggyback designs on top of a 4 mm and a 2.5 mm PENCIL™-type MAS rotor and stator have been realized allowing spinning speeds up to 15 and 25 kHz, respectively. The microrotors are machined to be inserted on top of a regular MAS rotor [Fig. 9(b)]. Rotor inner diameters are about 100, 120, or 140 μm and their length is 800 μm leaving sample volumes of 6, 10, and 12 nl respectively [Fig.

9(a)]. With the current design coil sizes were chosen to be at the limit of what can still be made by hand. Various proofs of principle experiments have been performed using this rotor design as will be described in Sec. VII.

For practical applications the best approach is to work with coil sizes adapted to the available sample amounts and, if necessary, the rf-field strength that is necessary to excite the spin system. The latter is of importance for spins experiencing very large linewidths or for the excitation and conversion of multiple-quantum coherences in, e.g., multiple-quantum magic angle spinning (MQMAS). A great advantage of the piggyback design is that the circuitry of the regular MAS probehead can remain intact. Therefore experiments can be performed simultaneously (or interleaved) in both micro- and macrorotor. This should be particularly easy to implement on modern spectrometers equipped with multiple receivers. Currently the macrorotor is used for quickly setting up the magic angle.

Very recently Sakellariou *et al.*[75] have introduced an interesting alternative for the implementation of microMAS. The idea is to spin a resonant *LC* microcoil circuit centered at the *inside* of a commercial MAS probehead relying on the inductive coupling between the microcoil and the large coil of the MAS probehead. In the so-called overcoupling regime all power send to the external coil is dissipated in the microcoil so the full advantage of downsizing the coil is maintained in rf field generation. This technology has specific advantages for the study of hazardous materials that need confinement for safety reasons such as the study of radioactive materials. Furthermore rotation of the coil is advantageous in averaging susceptibility effects. Disadvantages are eddy currents that occur in the coil due to the rotation which can cause heating and generates noise although they proved to be minor for the coil size used (750 μm). Devising an efficient doubly tuned circuit is far from trivial, however.

VII. EXPERIMENTAL IMPLEMENTATION AND APPLICATION

As was recently reviewed by Webb[49] in liquid-state NMR different probe designs with active sample volumes ranging from several nanoliters to microliters have been realized using either solenoid coils wound around capillaries or lithographically produced planar coils. With the latter techniques it is easier to go to smaller sample volumes and use the advantageous features of microfluidic devices at the expense of spectral resolution. Most applied studies have been performed in the 1–10 μl regime using capillary probeheads.[51] Also a number of hyphenated probes have been developed combining NMR with chemical separation techniques allowing the unambiguous identification of very small amounts of materials.[56,57,90,59,91] To speed up analysis probes with parallel arrangements of microcoils have been built.[90,92] Besides analytical applications it has been demonstrated that structural elucidation of proteins which are available only in nanomole quantities is feasible.[93] In MRI microcoils have been used to image single cells and obtain localized spectra from individual neurons. Here, besides sensitivity, diffusion in living tissue is an additional issue affecting the ultimate resolution.[94]

Although small coils have been used occasionally in magnetic resonance studies at high-field magnet laboratories, their use in mainstream solid-state NMR has not been explored extensively. Besides our work[64–67] we are aware only of the recent work of Sakellariou *et al.*[75] and an applied study on silk fibers by Yamauchi *et al.*[78] Here we review this work and show recent advances in microMAS probe technology and microfluidics.

A. Powdered samples

The majority of samples studied by solid-state NMR are powders or orientationally disordered in another way, e.g., as in a glass. This means that in general there is no obvious sample geometry that needs to be considered in the coil design. In that case the solenoid is a suitable detector geometry. For static NMR experiments on powdered samples solenoid microcoil probeheads were developed with an inner diameter of 300–400 μm using the integrated coil-capacitor design.[64] The performance, in terms of sensitivity and rf characteristics, of these probeheads was studied for ^{1}H, ^{31}P, and ^{27}Al in different model compounds in view of the feasibility of specific applications. The results show that the LOD is approximately 10^{14} spins/$\sqrt{}$Hz.

A specific advantage of microcoils for solid-state NMR applications is that they can generate extremely high rf fields if implemented in appropriate circuits. Using a rf power of 270 W for protons at 400 MHz (9.4 T) a record B_1-field strength of 4.7 MHz was achieved. For aluminum at 156 MHz (14.1 T) a 1.9 MHz B_1-field was realized using 380 W of rf power in a narrow band probehead, and 3 MHz at 850 W power proved possible in a slightly smaller diameter broadband probe. This allows the excitation of spectra of nuclei whose resonance lines are dispersed over several megahertz. This is particularly useful for quadrupolar nuclei experiencing large quadrupolar interactions as was demonstrated for ^{27}Al in a 30 μg powder sample of sapphire where the intensities in the quadrupolar satellites are dispersed over 720 kHz, but are clearly observed without significant distortions, reflecting the features of a site with C_{QCC}=2.4 MHz and η=0 (Ref. 64, Fig. 6). So in this case a nonselective excitation of the spin system proved possible. For quadrupolar nuclei in general, the choice for selectively exciting a single transition or nonselective excitation of the entire spin system is an extra consideration to be made when trying to obtain useful spectra. This is also important when implementing sensitivity enhancement techniques such as double frequency sweeps[95] and/or (quadrupolar) Carr Purcell Meiboom Gill (CPMG).[96,97] Situations where the rf-field strength and quadrupolar frequency are of similar magnitude can be exploited in nutation NMR.[98,99] Considering the high rf-field strengths that can be achieved, the microcoils realistically introduce the B_1-field strength as an extra parameter in designing experiments. This should help us to "unlock" some nuclear spin species with large quadrupolar line broadening for NMR observation.

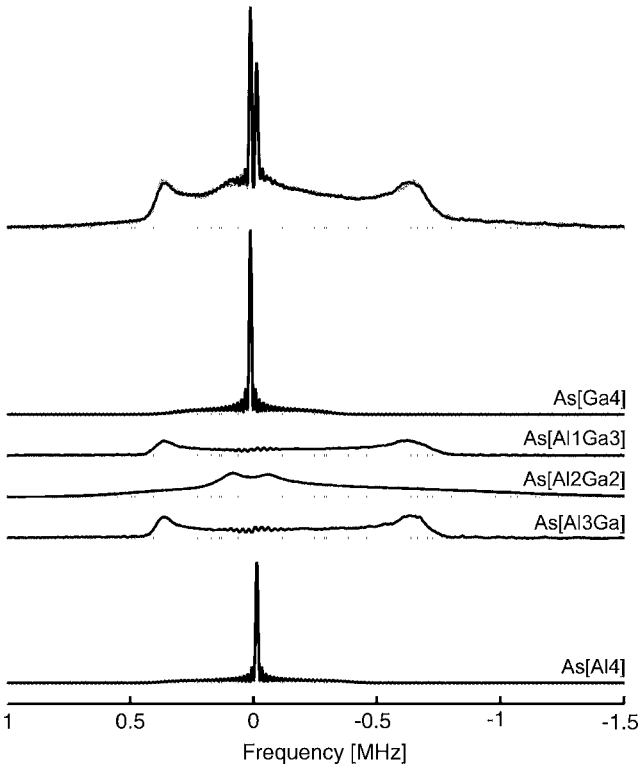

FIG. 10. Reconstructed ^{75}As NMR powder spectrum (dashed line) of $Al_{0.489}Ga_{0.511}As$ MOCVD grown films from a series of frequency-stepped (quadrupolar)CPMG experiments taken in a static probehead equipped with a 1.2 mm i.d. solenoid using a rf-field strength of 520 kHz and an external field of 18.8 T (800 MHz). The spectrum can be deconvoluted (solid lines) using genetic algorithms into five constituents assigned to the five different As coordinations of arsenic in the material. Quadrupolar coupling constants vary from 0.65 to 33.5 MHz leading to linewidth up to 2 MHz.

For the study of powdered solids with wide lines the optimal coil design is a balance between coil diameter in relation to the amount of sample that is available and secondly the rf-field strength that is needed to excite the full powder pattern. For example, currently we are involved in a multinuclear NMR study of $Al_xGa_{1-x}As$ samples. These samples are grown by metal-organic chemical vapor deposition (MOCVD) and typically of the order of 1 mg of sample is available. Especially ^{75}As NMR proves to be very difficult as ^{75}As with different Al and Ga coordination experiences enormously different quadrupolar interactions ranging from a few hundred kHz to more than 30 MHz, resulting in linewidths of more than 1 MHz even at 18.8 T. With an appropriate design of the tuning capacitor we can achieve rf fields between 500 kHz and 1 MHz for heteronuclei using coils of about 1 mm diameter, which allows us to effectively excite the entire spectrum while using the full sample that is available (Fig. 10).

To be considered a viable tool for studying solids, magic angle spinning needs to be implemented. Solid-state NMR has brought forth an extensive toolkit[100–103] of experiments relying on MAS to average anisotropic interactions that, if desired, can be reintroduced by devising rotor-synchronized pulse sequences that interfere with the coherent averaging at specific times. This means that one can retain anisotropic information for complex materials while maintaining high-resolution detection needed to resolve the various structural

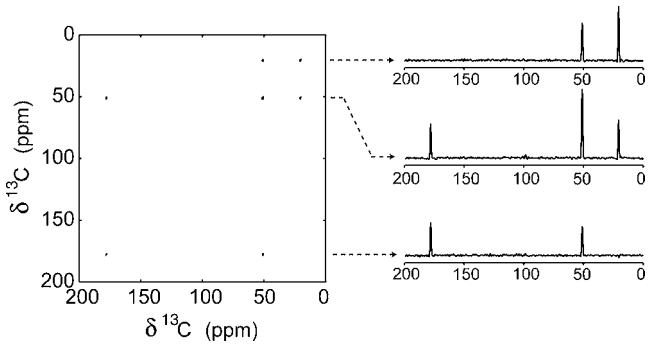

FIG. 11. Homonuclear $^{13}C-^{13}C$ correlation spectrum obtained for 6 nl uniformly enriched L-alanine. The experiment was performed acquiring 64 scans for 300 t_1 increments. The POST-C7 homonuclear recoupling sequence was applied with the sample spinning at 12 005 Hz. A clean spectrum is obtained with a good S/N ratio showing the expected cross peaks for the C′ and C^{α} and the C^{α} and C^{β} carbons.

sites in such a sample. As was described in Sec. VI we have implemented piggyback MAS designs,[65] based on the integrated microcoil-resonator circuit, with an active sample volume of 6–12 nl. The first probehead is a H*X* probehead for use at 14.1 T (^{1}H 600 MHz) based on a Chemagnetics 4 mm MAS stator allowing spinning speeds up to ~15 kHz. Various proofs of principle experiments were conducted for a number of aminoacids and small peptides. These experiments show that cross-polarization magic angle spinning (CP-MAS) experiments are readily obtained for enriched compounds in reasonable measurement times with identical resolution compared to regular CP-MAS experiments of these compounds. For example, a CP-MAS spectrum of 6 nL of uniformly ^{13}C-labeled trialanine spectrum gave an excellent spectrum in about 10 000 acquisitions (Ref. 65, Fig. 2). The probe efficiency can be judged from the rf-field strength that is obtained for a given transmitter power P ($B_1/\sqrt{P}$). For this probehead we obtained a proton decoupling field of 200 kHz at 1.35 W power. A first assessment of the sensitivity showed that this probe was not performing at the theoretical optimum. By improving on the circuit design (Fig. 8) and a slight decrease of the coil diameter, by eliminating the coil former, the probe efficiency was improved by a factor of 1.8 coming much closer to the sensitivity as predicted by Eq. (3). We determined the LOD (S/N=1 in 1 scan) for this probe by acquiring spectra for a 10 μg NaCl sample to be approximately 10^{14} spins/$\sqrt{\text{Hz}}$. Note that it is very difficult to get an accurate sample weight for these minute quantities mainly due to hydration effects. A nutation experiment performed at a rf-field strength of 870 kHz showed that the rf homogeneity of the coil is excellent with the signal amplitude decaying about 30% when going from a 90° to an 810° pulse ($A_{810}/A_{90}\sim 0.7$).

With this probe a spectrum of uniformly enriched alanine was obtained in 512 acquisitions resulting in a spectral S/N ratio of 210. In this case a decouple field of 240 kHz was obtained with 0.6 W of proton rf power. This sensitivity even makes it possible to perform two-dimensional NMR experiments as is shown in Fig. 11. A homonuclear $^{13}C-^{13}C$ correlation experiment was performed acquiring 64 scans for 300 t_1 increments. The POST-C7 homonuclear recoupling

sequence[104] was applied with the sample spinning at 12 005 Hz. A clean spectrum is obtained with a good S/N ratio showing the expected cross peaks for the C′ and C^{α} and the C^{α} and C^{β} carbons. As the sample was fully enriched, spinning at 12 kHz and using cw decoupling the linewidth is dominated by homonuclear carbon dipolar interactions and *J*-couplings[105] giving linewidths of the order of 100 Hz.

As in the case of the static probes, besides offering a very high mass sensitivity, the microMAS probes can generate extremely high rf-field strengths that can be put to good use, e.g., for exciting spins dispersed over large bandwidths, but also for decoupling purposes. It is well known that cw decoupling is not very efficient in getting high resolution especially with increasing spinning speed. The general idea is that MAS interferes with the decoupling scheme as the timescales of both averaging mechanisms are not sufficiently different. However, as detailed studies by Emsley and co-workers[106,107] show, the situation is much more complex as it involves the dynamics of strongly coupled many proton systems. As described by Sachleben *et al.*[106] even in the case of static samples different decoupling effects can be observed depending on the experimental conditions and the size of the spin system. A simplified account is as follows: first of all at low decoupler strength it is not possible to irradiate all spins on resonance and as a result (unresolved) line splittings occur from the remaining scaled dipolar interactions leading to line broadening. A different effect is predicted for "on-resonance" decoupling; at lower decoupler field strength intensity is lost to broad, generally invisible, decoupling sidebands. With increasing decoupling field these sidebands diminish and the intensity of the central line increases *without* changing its linewidth. Although MAS complicates matters by modulating all anisotropic interactions similar observations are made for spinning samples.[107] This means that with increasing rf-field strength cw decoupling should give narrow lines and increased signal intensities without the need of phase modulated decoupling sequences such as TPPM,[108] XiX,[109,110] or RN_n^v (Refs. 111 and 112) sequences. So far this could not be tested for realistic organic solids, however, because of the limited decoupling fields in commercial MAS probeheads.

In the microMAS probeheads decoupling fields in excess of 600 kHz are easily achieved without compromising the probehead. As was shown in Ref. 65 increasing the proton decoupling field from 100 to 600 kHz in cw decoupling experiments has marked effects on the ^{13}C CP-MAS spectrum of trialanine; clear line narrowing is observed together with an increased amplitude as the field strength increases. This effect only levels off at a decoupler field strength of 500 kHz. Although more detailed analysis is necessary the spectra seem to support the observations by de Paepe *et al.*,[107] namely, that the growth in signal intensity cannot be accounted for by the line narrowing alone. This would indicate that indeed at the highest field strength the on-resonance decoupling regime is reached. At this point the decoupling and spinning timescales differ by a factor of 50 from which one would expect interference effects to be minor.

Going to higher spinning speeds is very useful in many applications, e.g., when working with uniformly enriched samples or samples with abundant nuclei, high speeds are advantageous to effectively average homonuclear dipolar interactions. A piggyback microMAS probehead using a Chemagnetics 2.5 mm MAS is used to spin up to 25 kHz. This 9.4 T (^{1}H 400 MHz) probe, with rotor and coil dimensions identical to the previous one, shows impressive numbers for the coil sensitivity as can be judged from the rf-field

TABLE I. rf-field strength obtained at different power levels for protons and carbons in a 400 MHz piggyback microMAS H*X* probehead equipped with a 220 μm (inner diameter) solenoid coil.

H power (W)	^{1}H ν_1 (kHz)
0.10	98
0.43	230
1.5	475
6.2	1000
10.2	1290
X power (W)	^{13}C ν_1 (kHz)
0.10	32
0.50	71
1.8	148
5.6	300
9.4	385

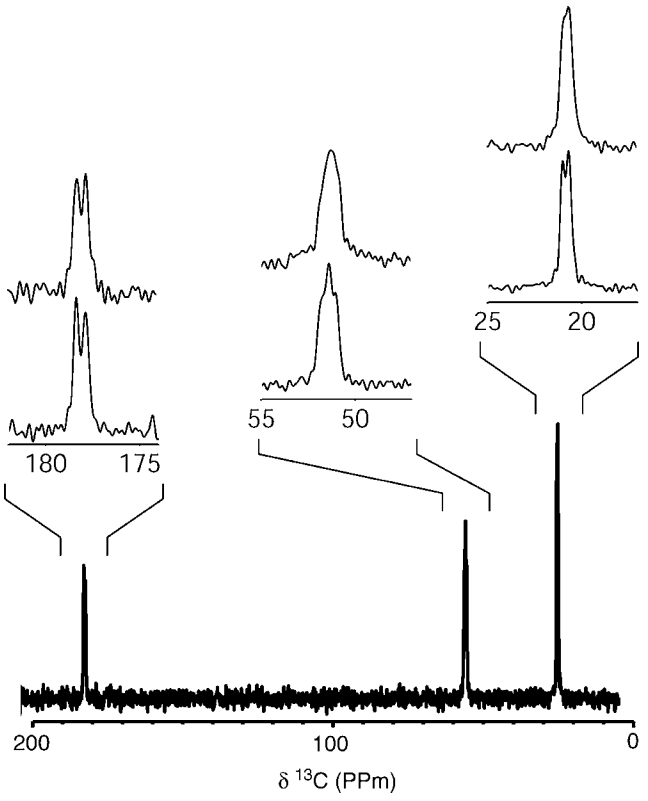

FIG. 12. ^{13}C CP-MAS spectrum obtained for 6 nl uniformly enriched L-alanine spinning at 24 kHz. A ramped CP contact time of 1 ms was used with a ±−5% amplitude ramp on the proton channel around ν_1=144 kHz and a ^{13}C field of 120 kHz. With appropriate decoupling the homonuclear ^{13}C *J*-couplings can be read directly from the spectrum. The lower traces are obtained with XiX decoupling at a rf-field strength of 350 kHz. The upper traces were obtained using cw decoupling at 350 kHz.

strengths obtained at various power levels shown in Table I. A ^{13}C CP-MAS of 6 nl uniformly enriched alanine was taken employing a spinning speed of 24 kHz. The best resolution was obtained using XiX decoupling[109] at a rf-field strength of 350 kHz (Fig. 12). In this case a linewidth of approximately 37 and 34 Hz was obtained for the C′ and C^{β}, respectively. The homonuclear carbon-carbon *J*-couplings can now be directly read from the spectrum being $J(C^{\alpha}-C^{\beta})=33$ Hz and $J(C^{\alpha}-C')=50$ Hz in accordance with literature data.[105] In this case using cw decoupling at 350 kHz (needing only 1 W power) also achieved resolution of the carbon-carbon *J*-couplings although the linewidths were slightly bigger being ~45 Hz for both C^{β} and C′, indicating that cw decoupling is still not fully efficient. In fact, no resolution improvement (or amplitude increase) was observed going from 350 to 605 kHz decoupler power. Whether this is related to the higher spinning speed is an open question. Furthermore it should be noted that Antonijevic and Bodenhausen[113] found a linewidth of the order of 15 Hz in natural abundance alanine spinning accurately at the magic angle. It will be interesting to see what linewidth can be achieved by high-power proton decoupling, in combination with accurate setting of the magic angle, in relation to the T_2's that can be observed in these compounds using Hahn echo experiments.[107]

Besides studying organic compounds microMAS is interesting for studying inorganic materials with abundant spins such as ^{23}Na and ^{27}Al. Being close in frequency to ^{13}C the probe response is very similar and preliminary experiments on minerals and zeolites with a low Si/Al ratio show that good S/N spectra can be obtained in reasonable time. Again we think that the high rf-field strengths offered by the microcoils have advantageous consequences. One obvious option would be to use optimal rf-field strength to efficiently excite and convert triple-quantum coherences in MQMAS experiments so that clean spectra with undistorted lineshapes could be obtained even for sites with very large quadrupolar coupling constants. For Al sites with a C_{QCC} around 15 MHz a rf field of 700–800 kHz is calculated to be optimal, which can easily be generated in the microMAS probehead. There are many more interesting applications, e.g., recently there are a number of interesting approaches introduced to indirectly detect ^{14}N nuclei.[114,115] The lineshapes in the indirect dimension of these experiments do not reflect the complete powder ensemble, however, because this cannot be efficiently excited. The high rf fields available in the microcoils could remedy this situation.

An interesting application demonstrated by Sakellariou *et al.*[75] is that microMAS can be implemented in a high-resolution magic angle spinning (HRMAS) context to obtain well-resolved proton spectra from biological tissues. This could reduce the size of biopsies necessary for tissue profiling. Centrifugation effects are expected to be minimal because of the small sample diameters in relation to the spinning speeds. In this context it is worth to note the development of needle shape microcoils that can be applied for such analyses.[116]

B. Single crystals and partially oriented samples

From the early beginnings of NMR single crystal studies have been used to determine both the magnitude and orientation of the anisotropic interaction tensors in the solid state such as chemical shift, dipolar interaction, and quadrupolar interactions. For instance, a lot of knowledge about the magnitude and orientation of ^{13}C tensors in various structural units in organic molecules have been compiled via single crystal studies.[117] Although one can determine the size of dipolar interactions very well in powders, the determination of the orientation can be very useful to find the absolute orientation of certain chemical bonds in a crystal. Finally quadrupolar tensors have been studied a lot to get insight in the local symmetry around a certain nucleus (unfortunately there is no comprehensive review). Many different procedures and hardware solutions have been proposed over the years. The recent work by Vosegaard *et al.*[118] introduces efficient probes that address one of the main problems of single crystal NMR, being sensitivity, together with easy to use software to extract the tensor values from the crystal rotation patterns. For many materials crystals of sufficient size are not available. Using 2 mm i.d. rf coils Vosegaard *et al.* have shown that small crystals could be studied detecting abundant high gamma nuclei such as ^{31}P and ^{87}Rb.[119] For many compounds crystal sizes are well below a millimeter and therefore further miniaturization of the coil is beneficial, which again has the additional advantage of being capable of exciting spins dispersed over a very large bandwidth. As was shown in Ref. 64 ^{27}Al NMR of mineral crystals of only a few nanoliters is possible. For the natural mineral kyanite, an Al_2SiO_5 polymorph having four crystallographic different Al sites with quadrupolar coupling constants ranging from 3.8 to 10.1 MHz, all spin transitions could be monitored during a rotation of the crystal about a single axis. In this case the resonances belonging to the satellite transitions are distributed over a bandwidth of 4 MHz.

Besides these single crystal studies, NMR can also provide valuable structural information about partially oriented materials. Here, the solenoid geometry is particularly well suited to study fibers. Oriented fibers play an important role both in synthetic polymers and in biological materials such as fibrous proteins. With the known orientation of an interaction tensor within the molecular frame the study of (partially) oriented materials gives information about the orientation of the molecules with respect to the external structure of the material (e.g., fiber axis or membrane plane). Moreover the degree of order can be studied. Asakura *et al.* have shown that small samples (70 μg) of aligned silk fiber, with the glycines 1-^{13}C-enriched, can be studied using ^{13}C CP-MAS experiments.

NMR of single crystals and partially oriented samples does not have to be restricted to static experiments. MAS is possible as well, with the advantage that homonuclear dipolar interactions that often broaden static spectra can be averaged. As has been described by Maricq and Waugh,[120] magic angle spectra of (partially) oriented material maintain the anisotropic information as long as the rotation speed is lower than the size of the interaction. In that case spinning a crystal

at the magic angle gives a sideband pattern where the amplitudes and phases of the spinning sidebands vary as a function of the size and orientation of the tensor with respect to the rotor axis frame. Based on this knowledge, Spiess and coworkers implemented rotor-synchronized two-dimensional (2D) and three-dimensional NMR experiments[121,122] to study structure and order in partially oriented polymers. This approach has been used in a single crystal to determine the orientation of the ^{29}Si chemical shift tensor in forsterite.[123] More recently Gross *et al.* have shown that single crystal rotational echo double resonance (REDOR) experiments can be used to determine the three-dimensional orientation of heteronuclear bond vectors in an amino acid, as well as the crystal's orientation relative to the rotor frame.[124] Subsequently this was combined with Lee–Goldburg CP experiments to orient hydrogen bonds with respect to the C^{α}–N bond with the aim to generate structural information for proteins. In general restricting the orientational distribution in a sample by using single crystals or partially aligned materials brings an important simplification of the spectra that makes it possible to more directly interpret the anisotropic information contained in the MAS spectra. That such techniques are relatively little used is only because in general there are no samples of appropriate size available. MicroMAS might be able to fulfill the promise held by these techniques.

For half-integer quadrupolar nuclei fast spinning gives a very useful resolution enhancement of the spectra. Powder MAS spectra of these nuclei are broadened by the second-order quadrupolar interaction which is not averaged by spinning at the magic angle. By spinning single crystals these broadened lines can be avoided. This is, for instance, very useful for the study of aluminosilicates such as zeolites. Generally in zeolites there are various crystallographically different framework sites which can be occupied by aluminum. By the inherent structural disorder that is present in most zeolites the resonance lines are not only broadened by the second-order quadrupolar interaction but also their distinct features are blurred by distribution in the NMR parameters due to the disorder. Therefore mostly asymmetrically broadened but furthermore featureless lines are observed.[125] Sometimes MQMAS experiments improve resolution but very few samples give *T*-site resolution. In microMAS this can be achieved, however, as is demonstrated for mesolite.

Mesolite is a naturally occurring zeolite in the natrolite group with two structural framework sites which can be occupied by Al with Na^+ and Ca^{2+} present in the pores as charge-balancing cations.[126] Due to the structural disorder the ^{27}Al MAS spectrum is broad and featureless with a little shoulder at the high-field side [Fig. 13(a)]. An ^{27}Al microMAS spectrum of a needle-shaped ($60\times60\times700$ μm^3 $\sim$2.5 nl) single crystal of mesolite, obtained in 10 000 acquisitions, shows three resolved resonances with an approximate intensity distribution of 1:2:1. Although the spectrum resolves different sites, the linewidth is almost 3 ppm, reflecting the structural disorder in the sample leading to a distribution in chemical shift and/or quadrupolar interaction. For comparison a sheared MQMAS spectrum of mesolite is shown in Fig. 13(c). In this case three sites can be resolved as well, here a substantial linewidth of about 3 ppm exists in the isotropic dimension of the spectrum [Fig. 13(d)] supporting the conclusions from the single crystal data. Further work is needed to fully assign the different spectral lines and determine the size and orientation of the quadrupolar tensors by performing rotor-synchronized 2D experiments. An important bonus of the microMAS experiments is that they can

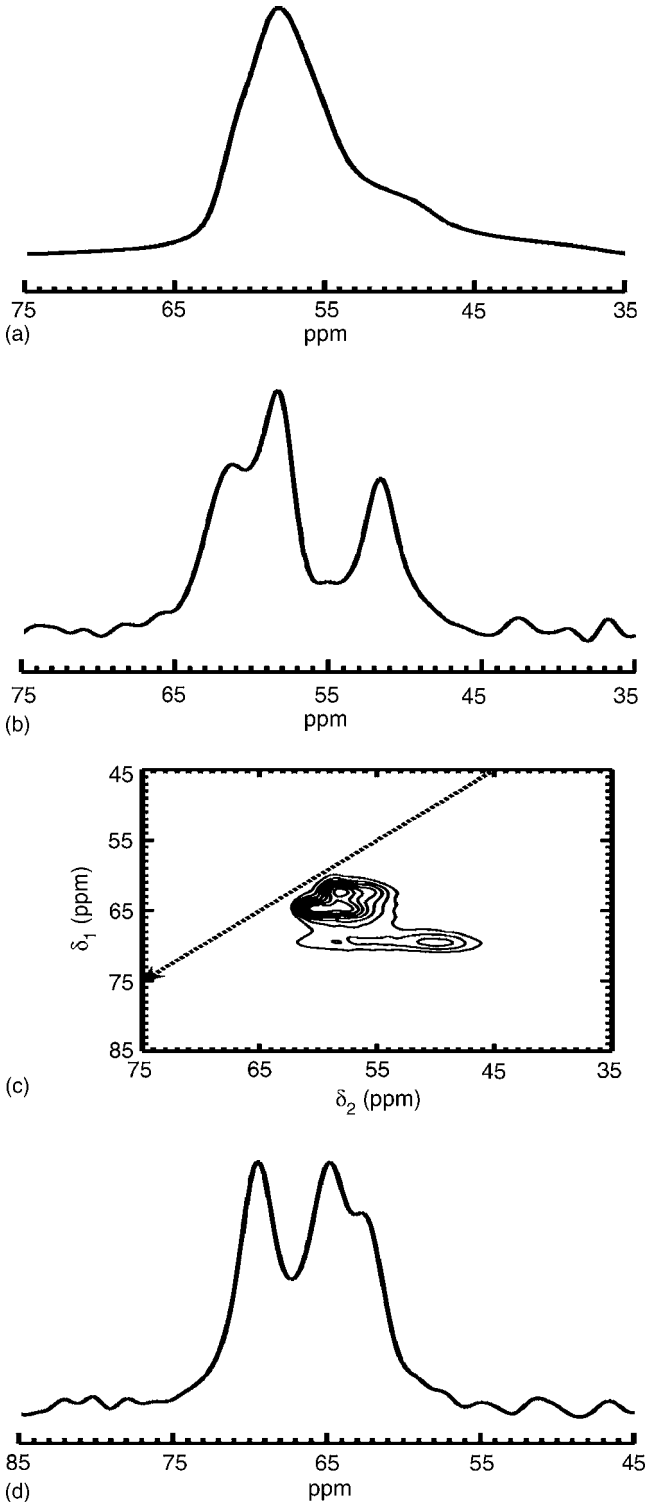

FIG. 13. (a) ^{27}Al MAS spectrum of a powdered mesolite sample. (b) ^{27}Al MAS spectrum of a needle-shaped ($60\times60\times700$ μm$^3\sim$2.5 nl) single crystal of mesolite, obtained in 10 000 acquisitions. (c) ^{27}Al sheared 3QMAS spectrum of powdered mesolite obtained by acquiring 180 scans for 128 t_1 increments. (d) F_1-projection of the 3QMAS spectrum in (c).

be interpreted quantitatively which allows obtaining the occupancy of the different sites in the zeolite lattice. This is very difficult to get from the MQMAS data. Furthermore it is worthwhile to notice that the microMAS experiment on the single crystals needed less than half the measurements for the triple-quantum magic angle spinning (3QMAS) experiment on the powdered sample. A full study of various zeolites is underway.

C. Thin films

NMR studies of thin films have been restricted to situations where many films could be stacked into a sample of macroscopic thickness as can be done for membranes prepared on thin glass plates. This makes it possible to study the structure, orientation, and mobility of membrane proteins.[127] Another alternative is to obtain freestanding films which can be stacked or rolled or crushed as a powder to be inserted in a solenoid coil. To study thin films in their actual environment a flat detector coil is desired. As was explained in Sec. III the stripline geometry is favored in this case because of its high sensitivity and scalability to the actual sample dimensions. To explore this capability a 10 μm thick film of commercial polyethylene based packaging material, corresponding to a sample volume of ~10 nl, was placed over the stripline. A proton single-pulse excitation experiment gave a S/N ratio of 165 in as little as four scans (Ref. 67, Fig. 7). This proton wide-line spectrum can be deconvoluted in three typical components attributed to the rigid, semirigid, and soft amorphous phases of the polymer in accordance with literature data on polyethylene.[128] This result demonstrates the sensitivity of the stripline for thin-film NMR spectroscopy. An application we aim for is to support the search for lightweight metal hydride storage materials. As is shown by Dam *et al.*[129] a thin-film combinatorial chemistry approach is a viable method to identify new hydrogen storage materials. This method could benefit tremendously from NMR if the hydrogen density and mobility could be visualized. To explore this possibility a proton Hahn-solid-Hahn echo experiment[130] for 5 nl of $NaAlH_4$ was dispersed as a powder onto the stripline under ambient conditions. The spectrum appears to be compatible with the observations in bulk material, consisting of a 42.2 kHz broad line attributed to $NaAlH_4$. A second narrower compound builds up during the experiments probably due to hydration/oxidation of the sample. These experiments indicate that the stripline configuration might be exploited for highly resolved materials imaging of hydrogen storage materials and other compounds grown in thin-film configurations.

D. Microfluidics

The development of flat microcoils has mainly been driven by the possibility to integrate them into microfluidic devices with the aim to add NMR as a key analysis technique in the developing "lab on a chip" approach. The growing interest in small volume chemistry performed in dedicated chip sets demands analytical methods that can handle the corresponding volumes. Trumbull *et al.*[53] were the first to address this issue. Making a single turn planar coil they succeeded in getting well-resolved (1.4–3 Hz) spectra for approximately 400 nl of water and ethanol. Sensitivity appeared to be relatively poor, however. Using two- and three-turn flat helical coils Massin *et al.*[54] succeeded in increasing the sensitivity by an order of magnitude at the expense of spectral resolution by the same number. Wensink *et al.*[55] managed to improve both sensitivity and resolution with a flat helical coil, operating at very low field (1.4 T), above a straight microfluidic channel. From our analysis of the stripline geometry[66,67] we concluded that this would not only be able to improve on sensitivity but more importantly on resolution as susceptibility broadening can be avoided to a large extent due to the symmetry of the design as is explained in Sec. III. In a prototype probe we were able to demonstrate the sensitivity of the stripline design detecting 12 nl ethanol in a single scan. The LOD was determined to be 2.5×10^{13} spins/$\sqrt{}$Hz. Unfortunately resolution was flawed as the probe was built with solids applications in mind. Recently a fully integrated stripline design that achieves tremendous resolution was finished, as is shown in Fig. 14. A 600 MHz proton spectrum of 600 nl ethanol was obtained under flowing conditions in a single scan. Most impressive is the resolution of 1 Hz which allows resolving the proton *J*-multiplets down to the baseline. The chip is made from silicon where surface charges induce some losses resulting in a lowering of the Q of the resonator. As a result sensitivity is somewhat reduced with respect to theoretical prediction. Further optimizations of the production process are underway. A nutation experiment performed at a rf-field strength of 62 kHz (at 5 W rf power) shows the excellent rf homogeneity of the stripline design with an A_{810}/A_{90} ratio of 0.8. The related microslot design introduced by Maguire *et al.* also shows favorable numbers for sensitivity and resolution. As the rf field is not confined, the rf homogeneity is poorer, however. Considering the successful implementation of the microfluidic chip with stripline detector a probehead that allows the placement of a microfluidic reactor close to the NMR chip was built. Kinetic studies of a series of on chip reactions, such as Diels–Alder reactions, alcohol protections, and oxidation reactions are underway.

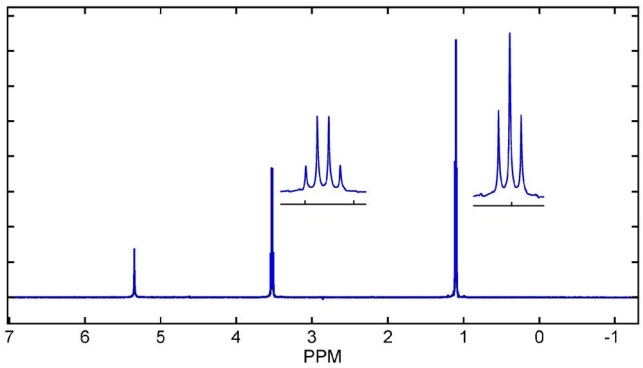

FIG. 14. (Color online) Single scan ^{1}H spectrum of a 600 nl ethanol sample (analytical grade) obtained in a microfluidic stripline probe. The signal-to-noise ratio is ~5050 and the resolution better than 1 Hz. The insets show that the proton *J*-multiplets are resolved down to the baseline.

VIII. CONCLUSIONS AND OUTLOOK

Recent developments in the miniaturization of radiofrequency coils and appropriate concepts to spin microscopic samples at high speed around the magic angle have made it possible to get NMR spectra of samples which are available only in microgram quantities. Solenoid coils with diameters down to a few hundred of microns make it possible to acquire both static and MAS spectra of nanoliters of material. Besides their high mass sensitivity, the tremendous rf fields offered by these coils can be efficiently exploited to excite spectra with resonances dispersed over very large bandwidths and allow effective decoupling schemes. In general the rf-field strength is added as a realistic design parameter in devising NMR experiments for, e.g., quadrupolar nuclei or paramagnetic systems. Alternatively microcoils make it possible to work with very low rf powers while still generating rf fields comparable to current NMR probe technology. This is one step in the way to low-cost possible tabletop NMR equipment discarding the need for high-power rf amplifiers. An additional advantage of the piggyback microMAS design is that the supporting "macroMAS" setup remains intact which makes it possible to run experiments simultaneously or in an interleaved way.

Moving to flat detector coils opens the way for thin-film analyses by NMR, where the films can be studied in their actual setting without additional sample preparation steps. The stripline geometry proves to be the favorable design for this type of application, combining a very high sensitivity and resolution with a full scalability to the sample dimensions. Moreover the stripline should be favorable in avoiding E-field induced sample heating in conducting samples. The stripline concept also allowed a breakthrough for the integration of NMR in a microfluidic context; with this design there is no longer a trade-off between sensitivity and resolution.

It can be concluded that, although still in its early stages of development, microcoil NMR will open the way for many novel applications in NMR. It should be realized, however, that we are already close to reaching the theoretical limits for inductive detection. Therefore, further improvements of detector sensitivity by orders of magnitudes are not to be expected. A possible route to higher sensitivity is to cool coil and/or sample to low temperatures. Cooling both sample and detector coil in a microMAS setup should prove to be much less demanding than in current cryoMAS probe technology. Further sensitivity enhancements must come from the implementation of polarization enhancement schemes such as dynamic nuclear polarization, parahydrogen based reactions, or the use of optically polarized noble gases. It should be noted that a miniaturized design may also have an impact on the feasibility of implementation of these techniques. For instance, the production of hyperpolarized molecules through reactions with para-H_2 could be implemented in an uncomplicated way in microfluidic devices as hydrogenation reactions on chip have been demonstrated. For DNP miniaturized devices allow the construction of microwave single mode resonant structures which in turn would greatly relax the demand for microwave power. It is therefore anticipated that the development of high-sensitivity micro-NMR technology will become a very lively research field in the coming decade.

ACKNOWLEDGMENTS

We acknowledge the support and feedback from J. W. M. van Os and G. E. Janssen. We thank E. Sweers for his craftsmanship in constructing the microMAS devices. Professor L. Meerts and D. Grimminck developed the wideline spectral deconvolution package for quadrupolar lineshapes. The Netherlands Organization for Scientific Research is acknowledged for financial support of this research through an NWO-TOP grant. The Advanced Chemical Technologies for Sustainability organization is thanked for a grant in the Process on a Chip program.

[1] A. W. Overhauser, Phys. Rev. **92**, 411 (1953).
[2] A. Abragam, *The Principles of Nuclear Magnetism* (Clarendon, Oxford, 1961).
[3] R. A. Wind, R. Lewis, H. Lock, and G. E. Maciel, Adv. Chem. Ser. **229**, 45 (1993).
[4] L. R. Becerra, G. J. Gerfen, R. J. Temkin, D. J. Singel, and R. G. Griffin, Phys. Rev. Lett. **71**, 3561 (1993).
[5] V. S. Bajaj, C. T. Farrar, I. Mastovsky, J. Vieregg, J. Bryant, B. Elena, K. E. Kreischer, R. J. Temkin, and R. G. Griffin, J. Magn. Reson. **160**, 85 (2003).
[6] G. J. Gerfen, L. R. Becerra, D. A. Hall, R. G. Griffin, R. J. Temkin, and D. J. Singel, J. Chem. Phys. **102**, 9494 (1995).
[7] C. T. Farrar, D. A. Hall, G. J. Gerfen, S. J. Inati, and R. G. Griffin, J. Chem. Phys. **114**, 4922 (2001).
[8] C. S. Song, K. N. Hu, C. G. Joo, T. M. Swager, and R. G. Griffin, J. Am. Chem. Soc. **128**, 11385 (2006).
[9] K. N. Hu, V. S. Bajaj, M. Rosay, and R. G. Griffin, J. Chem. Phys. **126**, 044512 (2007).
[10] J. H. Ardenkjacr-Larsen, B. Fridlund, A. Gram, G. Hansson, L. Hansson, M. H. Lerche, R. Servin, M. Thaning, and K. Golman, Proc. Natl. Acad. Sci. U.S.A. **100**, 10158 (2003).
[11] A. Henstra, T. S. Lin, J. Schmidt, and W. T. Wenckebach, Chem. Phys. Lett. **165**, 6 (1990).
[12] G. Buntkowsky, D. Stehlik, H. M. Vieth, and K. M. Salikhov, J. Phys.: Condens. Matter **3**, 6093 (1991).
[13] K. Takeda, K. Takegoshi, and T. Terao, J. Phys. Soc. Jpn. **73**, 2313 (2004); **73**, 2319 (2004).
[14] G. Lampel, Phys. Rev. Lett. **20**, 491 (1968).
[15] R. Tycko and J. A. Reimer, J. Phys. Chem. **100**, 13240 (1996).
[16] R. Tycko, Solid State Nucl. Magn. Reson. **11**, 1 (1998).
[17] J. Bargon, Helv. Chim. Acta **89**, 2082 (2006).
[18] R. Kaptein, Chem. Phys. Lett. **2**, 261 (1968); R. Kaptein and J. L. Oosterhoff, *ibid.* **4**, 195 (1969); **4**, 214 (1969).
[19] G. L. Closs, J. Am. Chem. Soc. **91**, 4552 (1969); G. L. Closs and A. D. Trifunac, *ibid.* **91**, 4554 (1969).
[20] J. Bargon, Photochem. Photobiol. Sci. **5**, 970 (2006).
[21] K. H. Mok and P. J. Hore, Methods **34**, 75 (2004).
[22] L. T. Kuhn and J. Bargon, *In Situ NMR Methods in Catalysis* (Springer, Berlin, 2007), Vol. 276, p. 125.
[23] M. G. Zysmilich and A. McDermott, J. Am. Chem. Soc. **116**, 8362 (1994); M. G. Zysmilich and A. McDermott, Proc. Natl. Acad. Sci. U.S.A. **93**, 6857 (1996); J. Am. Chem. Soc. **118**, 5867 (1996); A. McDermott, M. G. Zysmilich, and T. Polenova, Solid State Nucl. Magn. Reson. **11**, 21 (1998).
[24] J. Matysik, Alia, P. Gast, H. J. van Gorkom, A. J. Hoff, and H. J. M. de Groot, Proc. Natl. Acad. Sci. U.S.A. **97**, 9865 (2000).
[25] A. Diller, S. Prakash, A. Alia, P. Gast, J. Matysik, and G. Jeschke, J. Phys. Chem. B **111**, 10606 (2007).
[26] C. R. Bowers and D. P. Weitekamp, Phys. Rev. Lett. **57**, 2645 (1986); J. Am. Chem. Soc. **109**, 5541 (1987).
[27] M. G. Pravica and D. P. Weitekamp, Chem. Phys. Lett. **145**, 255 (1988).
[28] D. Canet, C. Aroulanda, P. Mutzenhardt, S. Aime, R. Gobetto, and F. Reineri, Concepts Magn. Reson. Part A **28**, 321 (2006).

[29] L. T. Kuhn and J. Bargon, *In Situ NMR Methods in Catalysis* (Springer, Berlin, 2007), Vol. 276, p. 25.
[30] P. Bhattacharya, K. Harris, A. P. Lin, M. Mansson, V. A. Norton, W. H. Perman, D. P. Weitekamp, and B. D. Ross, Magn. Reson. Mater. Phys., Biol., Med. **18**, 245 (2005).
[31] J. Haupt, Z. Naturforsch., A: Phys. Sci. **28**, 98 (1973); J. Haupt, Phys. Lett. **38**, 389 (1972); J. Haupt, Z. Naturforsch. A Astrophysik Physik Und Physikalische Chemie A **26**, 1578 (1971).
[32] P. Beckmann, S. Clough, J. W. Hennel, and J. R. Hill, J. Phys. C **10**, 729 (1977).
[33] B. Vanriet and L. Vangerven, Phys. Rev. B **26**, 2442 (1982).
[34] M. Tomaselli, U. Meier, and B. H. Meier, J. Chem. Phys. **120**, 4051 (2004); M. Tomaselli, C. Degen, and B. H. Meier, *ibid.* **118**, 8559 (2003).
[35] C. J. Jameson and A. C. Dedios, J. Chem. Phys. **97**, 417 (1992).
[36] J. L. Bonardet, J. Fraissard, A. Gedeon, and M. A. Springuel-Huet, Catal. Rev. - Sci. Eng. **41**, 115 (1999).
[37] T. Pietrass and H. C. Gaede, Adv. Mater. (Weinheim, Ger.) **7**, 826 (1995).
[38] A. Cherubini and A. Bifone, Prog. Nucl. Magn. Reson. Spectrosc. **42**, 1 (2003).
[39] Q. Wei, G. K. Seward, P. A. Hill, B. Patton, I. E. Dimitrov, N. N. Kuzma, and I. J. Dmochowski, J. Am. Chem. Soc. **128**, 13274 (2006).
[40] E. J. Ruiz, D. N. Sears, A. Pines, and C. J. Jameson, J. Am. Chem. Soc. **128**, 16980 (2006).
[41] M. S. Albert, G. D. Cates, B. Driehuys, W. Happer, B. Saam, C. S. Springer, and A. Wishnia, Nature (London) **370**, 199 (1994).
[42] D. A. Yablonskiy, A. L. Sukstanskii, J. C. Leawoods, D. S. Gierada, G. L. Bretthorst, S. S. Lefrak, J. D. Cooper, and M. S. Conradi, Proc. Natl. Acad. Sci. U.S.A. **99**, 3111 (2002).
[43] Y. Q. Song, Concepts Magn. Reson. **12**, 6 (2000).
[44] H. J. Jansch, P. Gerhard, M. Koch, and D. Stahl, Chem. Phys. Lett. **372**, 325 (2003).
[45] A. G. Webb, Prog. Nucl. Magn. Reson. Spectrosc. **31**, 1 (1997).
[46] D. I. Hoult and R. E. Richards, J. Magn. Reson. (1969-1992) **24**, 71 (1976).
[47] N. A. Wu, T. L. Peck, A. G. Webb, R. L. Magin, and J. V. Sweedler, Anal. Chem. **66**, 3849 (1994).
[48] D. L. Olson, T. L. Peck, A. G. Webb, R. L. Magin, and J. V. Sweedler, Science **270**, 1967 (1995).
[49] A. G. Webb, J. Pharm. Biomed. Anal **38**, 892 (2005).
[50] D. L. Olson, Anal. Chem. **76**, 2966 (2004).
[51] F. C. Schroeder and M. Gronquist, Angew. Chem., Int. Ed. **45**, 7122 (2006).
[52] J. E. Stocker, T. L. Peck, A. G. Webb, M. Feng, and R. L. Magin, IEEE Trans. Biomed. Eng. **44**, 1122 (1997).
[53] J. D. Trumbull, I. K. Glasgow, D. J. Beebe, and R. L. Magin, IEEE Trans. Biomed. Eng. **47**, 3 (2000).
[54] C. Massin, F. Vincent, A. Homsy, K. Ehrmann, G. Boero, P. A. Besse, A. Daridon, E. Verpoorte, N. F. de Rooij, and R. S. Popovic, J. Magn. Reson. **164**, 242 (2003).
[55] H. Wensink, F. Benito-Lopez, D. C. Hermes, W. Verboom, H. Gardeniers, D. N. Reinhoudt, and A. van den Berg, Lab Chip **5**, 280 (2005).
[56] A. M. Wolters, D. A. Jayawickrama, and J. V. Sweedler, Curr. Opin. Chem. Biol. **6**, 711 (2002).
[57] D. A. Jayawickrama and J. V. Sweedler, J. Chromatogr., A **1000**, 819 (2003).
[58] K. Albert, Nachrichten Aus Der Chemie **54**, 428 (2006).
[59] M. D. Grynbaum, D. Kreidler, J. Rehbein, A. Purea, P. Schuler, W. Schaal, H. Czesla, A. Webb, V. Schurig, and K. Albert, Anal. Chem. **79**, 2708 (2007).
[60] K. R. Minard and R. A. Wind, Concepts Magn. Reson. **13**, 128 (2001).
[61] K. R. Minard and R. A. Wind, Concepts Magn. Reson. **13**, 190 (2001).
[62] F. Engelke, Concepts Magn. Reson. **15**, 129 (2002).
[63] S. Eroglu, B. Gimi, B. Roman, G. Friedman, and R. L. Magin, Concepts Magn. Reson., Part B **17B**, 1 (2003).
[64] K. Yamauchi, J. W. G. Janssen, and A. P. M. Kentgens, J. Magn. Reson. **167**, 87 (2004).
[65] H. Janssen, A. Brinkmann, E. R. H. van Eck, P. L. M. van Bentum, and A. P. M. Kentgens, J. Am. Chem. Soc. **128**, 8722 (2006).
[66] P. J. M. van Bentum, J. W. G. Janssen, and P. M. Kentgens, Analyst (Cambridge, U.K.) **129**, 793 (2004).
[67] P. J. M. van Bentum, J. W. G. Janssen, A. P. M. Kentgens, J. Bart, and J. G. E. Gardeniers, J. Magn. Reson. **189**, 104 (2007).
[68] D. I. Hoult, in *Encyclopedia of Nuclear Magnetic Resonance*, edited by D. M. Grant and R. K. Harris (Wiley, New York, 1996), p. 4256.
[69] D. I. Hoult, Concepts Magn. Reson. **12**, 173 (2000).
[70] D. Horne, R. D. Kendrick, and C. S. Yannoni, J. Magn. Reson. (1969-1992) **52**, 299 (1983).
[71] D. L. Olson, M. E. Lacey, and J. V. Sweedler, Anal. Chem. **70**, 645 (1998).
[72] A. C. Wright, T. A. Neideen, R. L. Magin, and J. A. Norcross, Rev. Sci. Instrum. **69**, 3938 (1998).
[73] D. A. Seeber, L. Ciobanu, and C. H. Pennington, Appl. Magn. Reson. **22**, 139 (2002); D. A. Seeber, R. L. Cooper, L. Ciobanu, and C. H. Pennington, Rev. Sci. Instrum. **72**, 2171 (2001).
[74] M. Kakuta, D. A. Jayawickrama, A. M. Wolters, A. Manz, and J. V. Sweedler, Anal. Chem. **75**, 956 (2003).
[75] D. Sakellariou, G. Le Gofi, and J. F. Jacquinot, Nature (London) **447**, 694 (2007).
[76] A. F. McDowell and N. L. Adolphi, J. Magn. Reson. **188**, 74 (2007).
[77] T. L. Peck, R. L. Magin, and P. C. Lauterbur, J. Magn. Reson., Ser. B **108**, 114 (1995).
[78] K. Yamauchi, T. Imada, and T. Asakura, J. Phys. Chem. B **109**, 17689 (2005).
[79] N. C. Nielsen, P. Daugaard, V. Langer, J. K. Thomsen, S. Nielsen, O. W. Sorensen, and H. J. Jakobsen, J. Biomol. NMR **5**, 311 (1995).
[80] P. E. Gor'kov, E. Y. Chekmenev, R. Q. Eu, J. Hu, T. A. Cross, M. Cotten, and W. W. Brey, J. Magn. Reson. **181**, 9 (2006).
[81] K. Woelk, J. Magn. Reson. **146**, 157 (2000).
[82] D. Canet, Prog. Nucl. Magn. Reson. Spectrosc. **30**, 101 (1997).
[83] I. Ardelean and R. Kimmich, Isr. J. Chem. **43**, 9 (2003).
[84] X. L. Zhang, K. Ugurbil, and W. Chen, Magn. Reson. Med. **46**, 443 (2001).
[85] Y. Maguire, I. L. Chuang, S. G. Zhang, and N. Gershenfeld, Proc. Natl. Acad. Sci. U.S.A. **104**, 9198 (2007).
[86] F. D. Doty, G. Entzminger, and Y. A. Yang, Concepts Magn. Reson. **10**, 327 (1998); **10**, 329 (1998).
[87] E. R. Andrew, A. Bradbury, and R. G. Eades, Nature (London) **182**, 1659 (1958).
[88] I. J. Lowe, Phys. Rev. Lett. **2**, 285 (1959).
[89] A. Samoson, T. Tuherm, J. Past, A. Reinhold, T. Anupold, and N. Heinmaa, *New Techniques in Solid-State NMR* (Springer, Berlin, 2005), Vol. 246, p. 15.
[90] A. M. Wolters, D. A. Jayawickrama, A. G. Webb, and J. W. Sweedler, Anal. Chem. **74**, 5550 (2002).
[91] M. D. Grynbaum, C. Meyer, K. Putzbach, J. Rehbein, and K. Albert, J. Chromatogr., A **1156**, 80 (2007); H. B. Xiao, M. Krucker, K. Putzbach, and K. Albert, *ibid.* **1067**, 135 (2005); K. Putzbach, M. Krucker, M. D. Grynbaum, P. Hentschel, A. G. Webb, and K. Albert, J. Pharm. Biomed. Anal **38**, 910 (2005); M. Krucker, A. Lienau, K. Putzbach, M. D. Grynbaum, P. Schuger, and K. Albert, Anal. Chem. **76**, 2623 (2004).
[92] H. Wang, L. Ciobanu, A. S. Edison, and A. G. Webb, J. Magn. Reson. **170**, 206 (2004); D. A. Jayawickrama and J. V. Sweedler, Anal. Chem. **76**, 4894 (2004); L. Ciobanu, D. A. Jayawickrama, X. Z. Zhang, A. G. Webb, and J. V. Sweedler, Angew. Chem., Int. Ed. **42**, 4669 (2003); Y. Li, A. M. Wolters, P. V. Malawey, J. V. Sweedler, and A. G. Webb, Anal. Chem. **71**, 4815 (1999).
[93] Y. Li, A. G. Webb, S. Saha, W. W. Brey, C. Zachariah, and A. S. Edison, Magn. Reson. Chem. **44**, 255 (2006).
[94] P. Glover and P. Mansfield, Rep. Prog. Phys. **65**, 1489 (2002).
[95] H. Schafer, D. Iuga, R. Verhagen, and A. P. M. Kentgens, J. Chem. Phys. **114**, 3073 (2001); D. Iuga, H. Schafer, R. Verhagen, and A. P. M. Kentgens, J. Magn. Reson. **147**, 192 (2000); A. P. M. Kentgens and R. Verhagen, Chem. Phys. Lett. **300**, 435 (1999).
[96] F. H. Larsen, J. Skibsted, H. J. Jakobsen, and N. C. Nielsen, J. Am. Chem. Soc. **122**, 7080 (2000); F. H. Larsen and N. C. Nielsen, J. Phys. Chem. A **103**, 10825 (1999).
[97] R. W. Schurko, I. Hung, and C. M. Widdifield, Chem. Phys. Lett. **379**, 1 (2003).
[98] A. Samoson and E. Lippmaa, J. Magn. Reson. (1969-1992) **79**, 255 (1988).
[99] A. P. M. Kentgens, Prog. Nucl. Magn. Reson. Spectrosc. **32**, 141 (1998).
[100] S. Dusold and A. Sebald, *Annual Reports on NMR Spectroscopy* (Academic, San Diego, 2000), Vol. 41, p. 185.
[101] S. P. Brown and H. W. Spiess, Chem. Rev. (Washington, D.C.) **101**, 4125 (2001).
[102] D. D. Laws, H. M. L. Bitter, and A. Jerschow, Angew. Chem., Int. Ed. **41**, 3096 (2002).

[103] I. Schnell, Current Analytical Chemistry **1**, 3 (2005).
[104] M. Hohwy, H. J. Jakobsen, M. Eden, M. H. Levitt, and N. C. Nielsen, J. Chem. Phys. **108**, 2686 (1998).
[105] T. I. Igumenova and A. E. McDermott, J. Magn. Reson. **164**, 270 (2003).
[106] J. R. Sachleben, S. Caldarelli, and L. Emsley, J. Chem. Phys. **104**, 2518 (1996).
[107] G. De Paepe, A. Lesage, and L. Emsley, J. Chem. Phys. **119**, 4833 (2003).
[108] A. E. Bennett, C. M. Rienstra, M. Auger, K. V. Lakshmi, and R. G. Griffin, J. Chem. Phys. **103**, 6951 (1995).
[109] A. Detken, E. H. Hardy, M. Ernst, and B. H. Meier, Chem. Phys. Lett. **356**, 298 (2002).
[110] P. Tekely, P. Palmas, and D. Canet, J. Magn. Reson., Ser. A **107**, 129 (1994).
[111] M. Carravetta, M. Eden, X. Zhao, A. Brinkmann, and M. H. Levitt, Chem. Phys. Lett. **321**, 205 (2000).
[112] M. H. Levitt, in *Encyclopedia of Nuclear Magnetic Resonance*, edited by D. M. Grant and R. K. Harris (John Wiley & Sons Ltd., Chichester, 2002), Vol. 9, p. 165.
[113] S. Antonijevic and G. Bodenhausen, Angew. Chem., Int. Ed. **44**, 2935 (2005).
[114] S. Cavadini, A. Abraham, and G. Bodenhausen, Chem. Phys. Lett. **445**, 1 (2007); S. Cavadini, S. Antonijevic, A. Lupulescu, and G. Bodenhausen, ChemPhysChem **8**, 1363 (2007).
[115] Z. H. Gan, J. P. Amoureux, and J. Trebosc, Chem. Phys. Lett. **435**, 163 (2007); Z. H. Gan, J. Magn. Reson. **184**, 39 (2007).
[116] R. R. A. Syms, M. M. Ahmad, I. R. Young, D. J. Gilderdale, and D. J. Collins, J. Micromech. Microeng. **16**, 2755 (2006).
[117] W. S. Veeman, Prog. Nucl. Magn. Reson. Spectrosc. **16**, 193 (1984).
[118] T. Vosegaard, E. Hald, P. Daugaard, and H. J. Jakobsen, Rev. Sci. Instrum. **70**, 1771 (1999); T. Vosegaard, E. Hald, V. Langer, H. J. Skov, P. Daugaard, H. Bildsoe, and H. J. Jakobsen, J. Magn. Reson. **135**, 126 (1998).
[119] T. Vosegaard, P. Daugaard, E. Hald, and H. J. Jakobsen, J. Magn. Reson. **142**, 379 (2000).
[120] M. M. Maricq and J. S. Waugh, J. Chem. Phys. **70**, 3300 (1979).
[121] G. S. Harbison, V. D. Vogt, and H. W. Spiess, J. Chem. Phys. **86**, 1206 (1987).
[122] J. J. Titman, S. F. Delacroix, and H. W. Spiess, J. Chem. Phys. **98**, 3816 (1993).
[123] G. H. Kunath-Fandrei, L. Kelbauskas, D. Doring, H. Rager, and C. Jager, Phys. Chem. Miner. **26**, 55 (1998).
[124] B. J. Gross, J. M. Tanski, and A. E. McDermott, J. Magn. Reson. **176**, 223 (2005).
[125] A. P. M. Kentgens, Geoderma **80**, 271 (1997).
[126] P. S. Neuhoff, S. Kroeker, L. S. Du, T. Fridriksson, and J. F. Stebbins, Am. Mineral. **87**, 1307 (2002).
[127] B. Bechinger, C. Aisenbrey, and P. Bertani, Biochim. Biophys. Acta **1666**, 190 (2004).
[128] C. Hedesiu, D. E. Demco, R. Kleppinger, A. A. Buda, B. Blumich, K. Remerie, and V. M. Litvinov, Polymer **48**, 763 (2007).
[129] B. Dam, R. Gremaud, C. Broedersz, and R. Griessen, Scr. Mater. **56**, 853 (2007).
[130] K. Schmidt-Rohr, J. Magn. Reson. **131**, 209 (1998); K. Schmidt-Rohr, Macromolecules **29**, 3975 (1996).